

Alexey Popov

TiO₂ NANOPARTICLES AS UV PROTECTORS IN SKIN

FACULTY OF TECHNOLOGY,
DEPARTMENT OF ELECTRICAL AND INFORMATION ENGINEERING,
INFOTECH OULU,
UNIVERSITY OF OULU



ACTA UNIVERSITATIS OULUENSIS
C Technica 304

ALEXEY POPOV

**TiO₂ NANOPARTICLES AS
UV PROTECTORS IN SKIN**

Academic dissertation to be presented, with the assent of
the Faculty of Technology of the University of Oulu, for
public defence in Raahensali (Auditorium L10), Linnanmaa,
on November 21st, 2008, at 12 noon

OULUN YLIOPISTO, OULU 2008

Copyright © 2008
Acta Univ. Oul. C 304, 2008

Supervised by
Professor Risto Myllylä

Reviewed by
Professor Valery Tuchin
Professor Leonhard Zastrow

ISBN 978-951-42-8897-5 (Paperback)
ISBN 978-951-42-8898-2 (PDF)
<http://herkules.oulu.fi/isbn9789514288982/>
ISSN 0355-3213 (Printed)
ISSN 1796-2226 (Online)
<http://herkules.oulu.fi/issn03553213/>

Cover design
Raimo Ahonen

OULU UNIVERSITY PRESS
OULU 2008

Popov, Alexey, TiO₂ nanoparticles as UV protectors in skin

Faculty of Technology, Department of Electrical and Information Engineering, University of Oulu, P.O.Box 4500, FI-90014 University of Oulu, Finland; Infotech Oulu, University of Oulu, P.O.Box 4500, FI-90014 University of Oulu, Finland

Acta Univ. Oul. C 304, 2008

Oulu, Finland

Abstract

Protecting human skin against harmful UV radiation from the sun is an acute problem nowadays. Due to decreased thickness of the ozone layer, more UV light reaches the ground surface. This is one of the reasons of increased frequency of skin diseases. Titanium dioxide (TiO₂) nanoparticles are embedded with sunscreens into the skin to attenuate UV radiation through absorption and scattering. The effectiveness of the interaction between particles and UV light depends on nanoparticle sizes.

The aim of the study is to predict how the optical properties of the superficial layer of the human skin (stratum corneum) can be modified by means of nanoparticles, assuming that these particles are spheres and do not aggregate (this is achieved by application of some modern treatment techniques). In-depth distribution of TiO₂ particles embedded into the skin after multiple applications of sunscreens was determined experimentally using the tape-stripping technique. A computer code implementing the Monte Carlo method was developed to simulate photon migration within the 20- μ m thick horny layer partially filled with nano-sized TiO₂ spheres, 35–200 nm in diameter. Dependencies of UV radiation of two wavelengths (310 and 400 nm) absorbed by and totally reflected from, as well as transmitted through the horny layer on the size of TiO₂ particles were obtained and analyzed. Silicon nanoparticles of the same diameters were considered for comparison. The most attenuating particles were found for both cases.

The harmful side-effect of UV light absorption by TiO₂ particles is the generation of free radicals. Study of this phenomenon, using an electron paramagnetic resonance technique, was also carried out in this thesis. Comparison of the strength of the effect was done for two particle sizes administered onto either glass slides or porcine ear skin.

Keywords: free radicals, Monte Carlo simulations, nanoparticles, skin, stratum corneum, TiO₂, titanium dioxide, UV radiation

Acknowledgements

The study on protective properties of TiO₂ nanoparticles reported in this thesis was performed at the Optoelectronics and Measurement Techniques Laboratory of the University of Oulu.

First of all, I am grateful to Prof. Risto Myllylä for the supervision of my studies and arrangement of all necessary conditions for it.

My acknowledgement also goes to the personnel of the Laboratory (former and present): Mikhail Kirillin, Alexander Bykov, Matti Kinnunen, Errki Alarousu and Tuukka Prykäri. I thank them for their useful discussions and assistance.

I thank Prof. Alexander Priezzhev from M.V. Lomonosov Moscow State University (Russia) and Prof. Jürgen Lademann from Charité University Hospital (Germany) for fruitful discussions and collaboration. Prof. Lademann is also acknowledged for hosting me in his laboratory and for his assistance in using measurement equipment during my research visits to Berlin.

Special thanks go to Prof. Valery Tuchin from Saratov State University (Russia) and Prof. Leonhard Zastrow from Lancaster S.A.M. (Monaco) for reviewing my thesis and useful comments improved the manuscript. I would like to thank Nicholas Longhurst for checking English of the thesis.

I thank also Dr. Elena Zagainova from Institute of Applied Physics (Russia) for the TEM images of titanium dioxide particles.

I would like to thank my family who supported and encouraged me all these years during my stay in Finland.

Financial support from Infotech Oulu Graduate School, Tauno Tönningin säätiö, Tekniikan edistämissäätiö (all Finland) and Deutscher Akademischer Austauschdienst (Germany) is highly appreciated.

Oulu, September 2008

Alexey Popov

List of terms, symbols and abbreviations

3D	Three-dimensional
4-POBN	α -(4-Pyridyl-1-oxide)-N-butyl nitron
Al ₂ O ₃	Alumina
CO ₂	Carbon dioxide
COLIPA	European Cosmetic, Toiletry and Perfumery Association
CW	Continuous-wave
DMPO	5,5-Dimethyl-1-pyrroline-N-oxide
DNA	Deoxyribonucleic acid
DPPH	1,1-Diphenyl-2-picrylhydrazyl
EPR	Electron paramagnetic resonance
ESR	Electron spin resonance
FTIR spectroscopy	Fourier-transform infrared spectroscopy
H ₂ O	Water
HG	Henye-Greenstein
MCPT TM	Mechanochemical processing
NIR	Near infrared
NO	Nitric oxide
¹ O ₂	Singlet oxygen
O ₂	Oxygen
O ₂ ⁻	Superoxide
O ₃	Ozone
OCT	Optical coherence tomography
OH	Hydroxyl radical
PCA	3-Carboxy-2,2,5,5-tetramethylpyrrolidine-1-oxyl
RNA	Ribonucleic acid
ROS	Radical oxygen species
Si	Silicon
SiO ₂	Silica
SPF	Sun protection factor
TEM	Transmission electron microscopy
TEMPO	2,2,6,6-Tetramethylpiperidine-1-oxyl
Tempol	4-Hydroxy-2,2,6,6-tetramethylpiperidine-N-oxyl
TiO ₂	Titanium dioxide
UV	Ultraviolet
UVA	Ultraviolet-A fraction

UVB	Ultraviolet-B fraction
UVC	Ultraviolet-C fraction
VIS	Visible
ZnO	Zinc oxide
A	Absorbance
Ar ⁺	Argon ion
¹⁴ C	Carbon-14 isotope
C	Concentration
cm	Centimeter
cm ²	Square centimeter
cm ³	Cubic centimeter
<i>d</i>	Particle diameter
eV	Electron-volt
<i>g</i>	Scattering anisotropy factor
g	Gram
GHz	Gigahertz
h	Hour
<i>i</i>	Imaginary unit
<i>Im(n)</i>	Imaginary part of the refractive index
K	Degree Kelvin
kg	Kilogram
kHz	Kilohertz
km	Kilometer
<i>k_e</i>	Extraordinary imaginary part of the refractive index
<i>k_o</i>	Ordinary imaginary part of the refractive index
<i>k_p</i>	Imaginary part of the refractive index of a particle
<i>L</i>	Free pathlength
<i>l_{ph}</i>	Mean free pathlength of a photon
lg	Logarithm of the base 10
<i>M</i>	Total mass of particles within a strip
m ²	Square meter
mg	Milligram
min	Minute
ml	Milliliter
mm	Millimeter
mM	Millimol per liter

mT	Millitesla
mW	Milliwatt
n	Tape strip number
N	Number of particles
nm	Nanometer
n_m	Refractive index of the medium
n_o	Ordinary real part of the refractive index
n_e	Extraordinary real part of the refractive index
n_p	Real part of the refractive index of a particle
o/w	Oil-in-water
°C	Degree Celsius
$p_{HG}(\theta)$	Henyey-Greenstein scattering phase function
$p_{Mie}(\theta)$	Mie scattering phase function
p_s	Probability of scattering
Q_a	Relative light absorption efficiency factor
Q_s	Relative light scattering efficiency factor
$Re(n)$	Real part of the refractive index
Q_{ext}	Relative light extinction efficiency factor
R	Ratio of scattering coefficients of particles and a host medium with particles
^{35}S	Sulphur-35 isotope
s	Second
T	Transmittance
V	Volume of a strip
V_0	Volume of a particle
w/o	Water-in-oil
θ	Azimuthal angle
λ	Light wavelength
μ_a	Absorption coefficient
μg	Microgram
μl	Microliter
μm	Micrometer
μ_s	Scattering coefficient
ρ_0	Density
σ_a	Absorption cross-section
σ_g	Geometrical cross-section

σ_s
 φ

Scattering cross-section
Polar angle

List of original papers

- I Popov AP, Lademann J, Priezzhev AV & Myllylä R (2007) Reconstruction of stratum corneum profile of porcine ear skin after tape stripping using UV/VIS spectroscopy. Proc SPIE 6628: 66281S–1–6. DOI: 10.1117/12.729525.
- II Popov AP, Priezzhev AV, Lademann J & Myllylä R (2004) Manipulation of optical properties of human skin by light scattering nanoparticles of titanium dioxide. Proc SPIE 5578: 269–277. DOI: 10.1117/12.567423.
- III Popov AP, Priezzhev AV & Lademann J (2005) Control of optical properties of human skin by embedding light scattering nanoparticles. Proc SPIE 5850: 286–293. DOI: 10.1117/12.633742.
- IV Popov AP, Priezzhev AV, Lademann J & Myllylä R (2005) TiO₂ nanoparticles as an effective UV-B radiation skin-protective compound in sunscreens. J Phys D: Appl Phys 38: 2564–2570. DOI: 10.1088/0022-3727/38/15/006.
- V Popov AP, Lademann J, Priezzhev AV & Myllylä R (2005) Effect of size of TiO₂ nanoparticles embedded into stratum corneum on ultraviolet-A and ultraviolet-B sun-blocking properties of the skin. J Biomed Opt 10: 064037–1–9. DOI: 10.1117/1.2138017.
- VI Popov AP, Priezzhev AV, Lademann J & Myllylä R (2007) Effect of multiple scattering of light by titanium dioxide nanoparticles implanted into a superficial skin layer on radiation transmission in different wavelength ranges. Quantum Electron 37: 17–21. DOI: 10.1070/QE2007v037n01ABEH013461.
- VII Popov AP, Priezzhev AV, Lademann J & Myllylä R (2008) Monte Carlo calculations of UV protective properties of emulsions containing TiO₂, Si and SiO₂ nanoparticles. Proc. SPIE 7022: 702211–1–7. DOI: 10.1117/12.804096.

These papers are referred to in the text by Roman numerals I–VII.

In Paper I, the results of the stratum corneum reconstruction after tape stripping in experiments with porcine skin *in vitro* (ears of freshly slaughtered pigs) are compared with those carried out on humans *in vivo* (flexor forearm) taken from references.

Paper II describes a model of the stratum corneum with embedded TiO₂ nanoparticles based on experimental results and shows attenuation of 310- and 400-nm radiation obtained by Monte Carlo simulations.

Paper III continues the studies from Paper II and involves another UV wavelength, namely 290.5 nm, and different particle concentrations.

Paper IV applies the developed model and the Mie theory to reveal the most effective size of TiO₂ nanoparticles to attenuate UV radiation in the erythral peak.

In Paper V, nanoparticles of different sizes are considered and their effect on reflected, transmitted and absorbed UV radiation is investigated.

Paper VI implements studies on multiplicity of photon scattering within stratum corneum with nanoparticles and compares effects of particle administration for radiation from UVB, UVA and visible spectral ranges.

In Paper VII the effect of TiO₂, Si and SiO₂ nanoparticles embedded in a transparent emulsion on UV light attenuation is studied.

Contents

Abstract	
Acknowledgements	5
List of terms, symbols and abbreviations	7
List of original papers	11
Contents	13
1 Introduction	15
1.1 Motivation.....	15
1.2 Objectives.....	16
1.3 Outline of the thesis	16
2 Skin structure	19
2.1 Stratum corneum	20
2.2 Viable epidermis.....	21
2.3 Dermis	21
2.4 Hypodermis	21
3 Stratum corneum: structure and properties	23
3.1 Structure of stratum corneum	24
3.1.1 Water.....	24
3.1.2 Corneocytes	24
3.1.3 Intercellular lipids.....	24
3.2 Properties of stratum corneum	25
3.2.1 Permeability.....	25
3.2.2 Optical properties in UV range.....	26
4 Porcine and human skin: comparison	29
4.1 Penetration studies.....	29
4.2 Morphology and thickness	29
4.3 Tape stripping procedure	30
4.4 UV/VIS spectroscopy.....	31
4.5 Visualization of corneocytes	34
5 UV radiation	37
5.1 Solar spectrum.....	37
5.2 Effects on skin.....	37
5.3 Action spectrum and effective spectrum	38
6 Nanoparticles of titanium dioxide	41
7 Free radical generation under UV irradiation	43
7.1 Free radicals	43

7.2	EPR technique.....	43
7.3	Experiments with TiO ₂ nanoparticles.....	44
7.3.1	Raman spectroscopy.....	45
7.3.2	Mie calculations.....	46
7.3.3	Experiments on glass slides.....	47
7.3.4	Experiments on porcine skin in vitro.....	49
8	UV protection by nanoparticles	53
8.1	Multiple application of sunscreens on skin: location of particles	53
8.2	Mie calculations: cross-sections and anisotropy factors	55
8.3	Monte Carlo simulations	57
8.3.1	Model of stratum corneum with particles.....	57
8.3.2	Results of simulations.....	61
9	Summary	69
	References	71
	Original papers	79

1 Introduction

1.1 Motivation

Protecting human skin against the harmful influence of UV solar radiation, harm which includes such dangerous diseases as skin cancer is an acute problem (Diffey 1991). Conventionally, skin is considered a multi-layered medium (Tuchin 2000, Tuchin 2002). The outermost layer, called stratum corneum (or horny layer), serves as a natural barrier for deeper skin layers with living cells. From the optical viewpoint, its property is, in particular, to prevent penetration of UV radiation into the epidermis and dermis. In order to strengthen its protective functions, a variety of sunscreens containing chemical (absorbing) UV filters have been developed (Edlich *et al.* 2004). To increase the amount of backscattered UV radiation and avoid allergic reaction of individuals, chemical components are partially replaced nowadays by so-called ‘physical components’, nano-sized particles of titanium dioxide TiO_2 or zinc oxide ZnO (Innes *et al.* 2002). In addition to absorption (within the definite UV spectral region) they have pronounced scattering properties and decrease the amount of transmitted light through absorption and scattering.

The UV solar spectrum consists of three ranges: UVA (315–400 nm), UVB (280–315 nm), and UVC (100–280 nm) (McKinlay & Diffey 1987a). The most harmful rays from the UVC range are completely absorbed by the stratospheric ozone layer in the upper part of the Earth’s atmosphere, while the UVA and UVB fractions reach the ground surface. The effect of the UV radiation on human skin can be divided into two categories: acute and chronic (Diffey 1991). The former includes sunburn (caused by UVB) and sun-tanning (by UVA) as well as production of the vitamin D (caused by UVB). The chronic effects are carcinoma (by UVB), melanoma and photoaging (both by UVA). All the effects caused by the UVB radiation, except for the synthesis of the vitamin D, are negative. In the last decades, due to the depletion of the ozone layer, an increasing portion of UV penetrates the atmosphere. Another possible reason for larger doses of solar UV radiation reaching people is the greenhouse effect. The proposed climate change would make summers warmer, causing a corresponding change of behavior in people which results in their remaining longer outdoors (Diffey 2004).

However, not all the nanoparticles are equally effective (to attenuate UV radiation) for certain wavelengths of light. Moreover, the aggregation and agglomeration of particles in sunscreens reduce their protective properties. Some

emerging new manufacturing technologies which allow the production of nanopowders with a narrow size distribution and free from aggregation (Innes *et al.* 2002) will lead to better-quality sunscreens.

1.2 Objectives

The aim of the thesis is to consider how protective UV light properties of the uppermost layer of the skin, stratum corneum (horny layer) can be improved by the embedding of TiO₂ particles. This issue is investigated both experimentally and by Monte Carlo simulations. The Mie theory is applied to determine the most suitable sizes to attenuate UV radiation of specific wavelengths.

The second issue to consider is the side effect of the UV irradiation, namely, generation of free radicals. The contribution of skin and particles themselves to this effect is to be revealed.

1.3 Outline of the thesis

Chapter 2 of the thesis is devoted to the skin structure. The composition and function of the stratum corneum, viable epidermis, dermis and hypodermis are described.

Chapter 3 focuses on the structure and properties of the stratum corneum. The contents and role of its compounds, such as water, cells and lipids are discussed. The permeability and optical properties of the layer as a whole are represented. A review of the experimental methods used for the stratum corneum investigation is also given.

Chapter 4 compares human skin with porcine skin. Similarities resulting from experiments utilizing various techniques, e.g. tape stripping, UV/VIS spectroscopy, fluorescent microscopy are shown.

Chapter 5 contains information about UV radiation as a part of the solar spectrum. It shows the effect of the Earth's atmosphere on different UV fractions and their influence on skin.

Chapter 6 describes crystal structures and the properties of TiO₂ nanoparticles.

Chapter 7 introduces free radicals, reasons for their appearance and the electron paramagnetic resonance technique for their detection. The experimental part of the chapter describes the effects of TiO₂ nanoparticles of different sizes on radical formation under UV irradiation both on glass slides and porcine skin.

Chapter 8 describes a developed mathematical model of the stratum corneum partially filled with nanoparticles for Monte Carlo simulations. The Mie theory is considered to produce input parameters for the simulations. Particles of two types, TiO_2 and Si, are compared from the viewpoint of UV light attenuation.

Chapter 9 summarizes the obtained results.

2 Skin structure

Skin is one of the largest organs of the human body. Being in contact with the ambient medium, its function is to protect inner organs from different types of hazards: mechanical, chemical, temperature, optical, biological etc. It occupies an area of about 2 m² and has a weight of about 3 kg (up to 20 kg if fatty tissue is taken into account) for adult individuals (Mosteller 1987). The skin thickness depends on the region and varies between 1.5 and 4 mm (Fritch 1998).

The methods for studying skin structure are divided in two: invasive and non-invasive. The former includes, for example, biopsy, when skin samples are taken and then analyzed with a microscope. The latter are non-damaging techniques, often implying optical methods, which use non-ionizing radiation and suitable spatial resolution, e.g. optical coherence tomography (OCT) (Otberg *et al.* 2003; Otberg, Richter, Knüttel *et al.* 2004; Jacobi, Waibler *et al.* 2005; Lademann, Knüttel *et al.* 2005), laser scanning microscopy (Meyer *et al.* 2006; Teichmann *et al.* 2006; Rieger *et al.* 2007), and fluorescence imaging (Riemann *et al.* 2004).

The layers of skin (starting from the skin surface) are stratum corneum, viable epidermis, dermis and hypodermis (a layer of subcutaneous fat). Sweat glands, sebaceous glands and hair follicles are also considered as a part of skin. The structure of skin is represented in Fig. 1 (www.mydr.com.au). An image obtained by optical coherence tomography from a flexor forearm skin of a healthy 27-years-old male is given in Fig. 2. The layered structure is clearly seen.

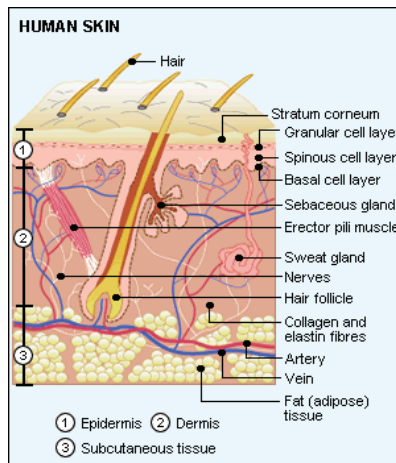


Fig. 1. Structure of skin (www.mydr.com.au).

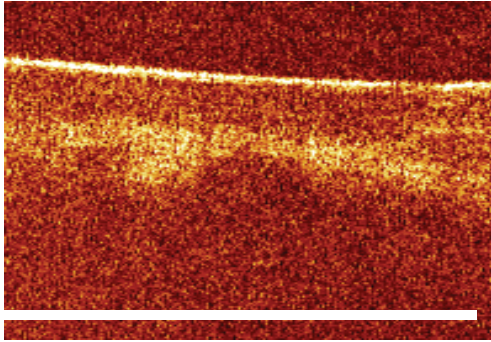


Fig. 2. An OCT image of human skin *in vivo* (flexor forearm). Scale: the bar at the bottom corresponds to 1 mm.

2.1 Stratum corneum

The outermost part of the skin is called the *stratum corneum* (horny layer). The published data concerning the thickness of the stratum corneum differ: 6–40 μm on such common areas as abdomen, flexor forearm, thigh, and back (Anderson & Cassidy 1973; Holbrook & Odland 1974).

The stratum corneum is formed by corneocytes – dead polyhedral-shaped cells without nuclei, approximately 40 μm in diameter and 0.5- μm -thick (Schaefer & Redelmeier 1996). Their cellular organelles and cytoplasm disappeared during the cornification process. There is an overlap between adjacent corneocytes which increases stratum corneum cohesion. The intercellular region is filled with lipid which represents a continuous medium and is required for barrier function.

The stratum corneum consists of about 15 layers, although exceeding this value significantly (5–10 times) in places of intensive use such as soles and palms. The upper layer (stratum disjunctum) contains about 3–5 layers and undergoes continuous desquamation. Water makes up 15% of its weight. The lower layer (stratum compactum) is thicker, more densely packed and more regular. Additionally, it is more hydrated than the stratum disjunctum (30%). The cells of stratum corneum renew themselves continuously: desquamated cells are replaced by “fresh” ones coming from the epidermis. One cell layer takes 24 hours to form, so the whole stratum corneum renews itself completely in two weeks.

2.2 Viable epidermis

The viable epidermis is located under the stratum corneum. Its thickness is about 100 μm . The epidermis comprises 10–20 layers of keratinizing epithelial cells, or *keratinocytes*, responsible for stratum corneum synthesis. This layer also contains melanocytes, which cause skin pigmentation and Langerhans cells which contribute to immune response. The viable epidermis is conventionally divided into three layers (counting from the dermis): stratum basale (basal layer), stratum spinosum (spinous layer), and stratum granulosum (granular layer). Such a division is caused by different stages of keratinocytes' evolution. The deepest of all of these, stratum basale, consists of stem cells and transit-amplifying cells. Committed cells detach from base membrane and move through the stratum spinosum and stratum granulosum towards the stratum corneum, changing their forms and contents. This migration process takes about 2–4 weeks.

2.3 Dermis

The dermis forms the largest part of the skin, with a thickness of 1200 μm . The most significant component of the layer is collagen fibers, accounting for 70% of the dermis weight. It forms a kind of skeleton within the dermis. The second important compound is elastic connective tissue, providing elasticity and shape retention. A variety of cell types is found in the layer: fibroblasts, endothelial and mast cells; microphages, lymphocytes and leukocytes can penetrate in case of inflammation. Fibroblasts produce connective tissue components such as collagen, laminin, fibronectin and vitronectin. Microphages play a role in phagocytosis and are important for protecting against microorganisms. Mast cells important in tissue regeneration after injury and in defence reactions against parasites. The dermis contains also blood plexus, which is responsible for such processes as nutrition, heat exchange, repair, immune responses and thermal regulations. Lymphatic vessels regulate pressure of the interstitial liquid in the dermis.

2.4 Hypodermis

The hypodermis is located under the dermis. It consists of fat cells (adipocytes) arranged in lobules. The role of this layer is to store energy and provide insulation and protection against injury. It may also serve as a reservoir of hydrophobic substances penetrating the stratum corneum.

3 Stratum corneum: structure and properties

In order to investigate the composition and structure of the stratum corneum, various techniques have been applied: fluorescent staining technique (Christophers 1971), X-ray (Bouwstra *et al.* 1995) and electron diffraction (Pilgram *et al.* 1998) spectroscopy, electron paramagnetic resonance (EPR) spectroscopy (Kawasaki *et al.* 1999), transepidermal water loss (TEWL) technique (Schwindt *et al.* 1998; Weigmann, Ulrich *et al.* 2005), tape stripping method (Weigmann *et al.* 1999), and attenuated total-reflectance Fourier-transform infrared (FTIR) spectroscopy (Garidel 2002).

A model of the stratum corneum accepted for percutaneous absorption is represented by “bricks in mortar”. Bricks are supposed to be protein-rich corneocytes, whereas intercellular lipids are seen as mortar. This model is simplified because the stratum corneum is not a homogeneous layer: its cells undergo morphological and chemical changes during their migration to the skin surface. Nevertheless, we will describe this layer as a whole. The structure of the stratum corneum is represented in Fig. 3 (Schaefer & Redelmeier 1996).

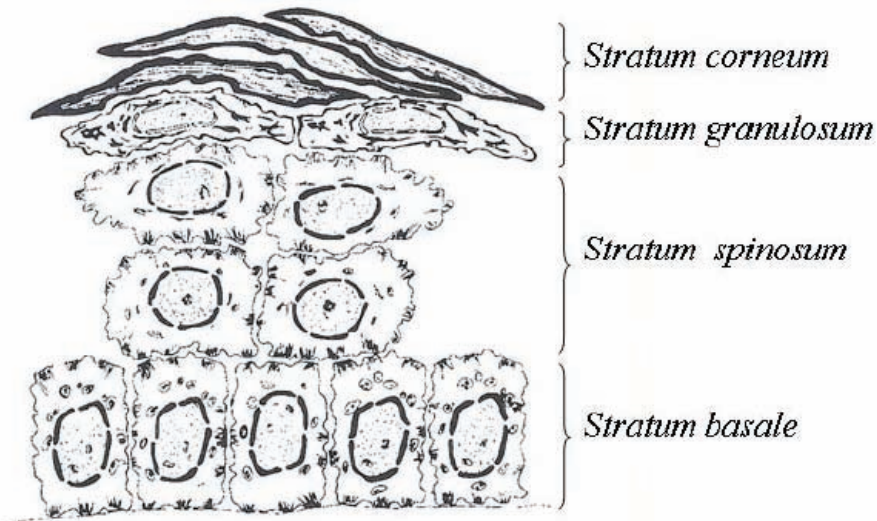


Fig. 3. Structure of the stratum corneum (Schaefer & Redelmeier 1996).

3.1 Structure of stratum corneum

3.1.1 Water

According to Schaefer & Redelmeier (1996), the stratum corneum consists of water (15%), proteins (70%) and lipids (15%). However, some authors (Bouwstra *et al.* 2003) report higher water content for the stratum corneum *in vivo*: 30–50%. It is not constant within the horny layer and increases with a depth reaching the water level of the epidermis (70% by weight). FTIR spectroscopy, combined with tape stripping (Bommannan *et al.* 1990) and cryo-scanning electron microscopy (Bouwstra *et al.* 2003) were used to determine water content in the stratum corneum at different hydration levels. Most of the water was accumulated in the corneocytes. At extremely high hydration levels (300% by weight), water domains were present also in intercellular regions. Between 17% and 300% by weight, the cell thickness increased linearly with water concentration suggesting that the swelling of the corneocytes occurred mainly in the direction perpendicular to the skin surface. Water content is not a constant value and it is influenced by air humidity, moisturizers, surfactants, and age.

3.1.2 Corneocytes

Corneocytes are the main storage for proteins in the stratum corneum. They contain a keratin core wrapped by an envelope. Protein composition is highly structured, insoluble and resistant to chemical and physical treatment.

The chemical composition of corneocytes can be sensed by FTIR spectroscopy. Identification of proteins can be revealed by amide I and amide II as well as by symmetric methyl absorption (Garidel 2002). The core of corneocytes consists mainly of highly-organized, densely packed keratins with some associated filaggrin. Keratins may be responsible for 80% of the dry mass of corneocytes.

A corneocyte envelope may occupy up to 7% of the dry mass of a corneocyte. The envelope is 90% proteins and 10% lipids (by mass). It is even more resistant to the effects of boiling, treatments of alkali and detergents than are the core proteins.

3.1.3 Intercellular lipids

Intercellular lipids as suggested by the name are located between corneocytes within the stratum corneum. They account for 15% of the dry mass of the layer.

They provide cohesion of corneocytes and are responsible for the barrier function of the stratum corneum. The lipids are chemically stable. Chemical composition is identified by methylene stretching vibrations and carbonyl ester band (Garidel 2002). It is accepted that the compounds of the lipids are ceramides, free fatty acids and cholesterol in equimolar concentrations. It was revealed that the lipids were organized in lamellae aligned parallel to the skin surface.

Lipids can exist in three forms: solid crystalline, gel and liquid crystal phase. The first two forms are characterized by orthorhombic and hexagonal hydrocarbon chain packing respectively. The difference between the packings can be monitored by means of diffraction (X-ray or electron) or by FTIR spectroscopy. In the model systems, one form can transform into another with a change in pressure, hydration, solvents, salt concentration, pH, temperature. The application of surfactants can also affect the fluidity of the intercellular lipids, which can be monitored by EPR spectroscopy, indicating the applied spin labels mobility. The transitions occur at the following temperatures: orthorhombic – hexagonal state at 30–45 °C; hexagonal – liquid crystal at 65–90 °C (Bouwstra *et al.* 1995).

3.2 Properties of stratum corneum

3.2.1 Permeability

Although the stratum corneum is a heterogeneous structure, in cases where there is liquid substance penetration, it behaves as a homogeneous membrane and the diffusion law is correct (Kalia *et al.* 1996; Kalia *et al.* 2000; Alberti *et al.* 2001). No indication of a tortuous pathway for water diffusing across the stratum corneum was found; the calculated diffusion pathlength was equal to the physical thickness of the layer (Schwindt *et al.* 1998). The penetration of substances can occur by intercellular (along lipid lamellae), by transcellular (through corneocytes) as well as via glands (sweat sebaceous) and along hairs. None of these ways can be treated exclusively.

The in-depth penetration profile of substances topically applied onto the skin is dependent on the vehicle used. In experiments with vanillin mixed with two kinds of emulsions, it was shown that the use of ethanol enhances penetration in comparison to w/o emulsion (Jacobi *et al.* 2003). Application of vehicles also affects the cohesion properties of corneocytes: o/w emulsion increases it and ethanol decreases it (Lademann *et al.* 2006).

Figure 4 illustrates an in-depth penetration profile of a chemical UV filter (used in sunscreens) reconstructed after tape stripping using spectroscopy methods. The concentration of the UV filter substance was determined for each tape strip, as described previously (Jacobi, Weigmann *et al.* 2004). The tape strips with corneocytes were cut to a size of $1.5 \times 4.3 \text{ cm}^2$. Then they were put into tubes containing 6.45 ml of ethanol each (UVASOL, Merck, Germany). The tubes were processed by ultrasound for 10 min (Sonorex Super RK 102H, Bandelin Electronic, Germany). Solutions were purified by centrifugation (5 min at 4000 cycles/s, MR 1812 centrifuge, Jouan, Germany). The uppermost part of the solution was transferred with a pipette into a quartz cell of 10 or 1 mm in thickness (Hellma, Germany). The UV/VIS spectra of the extracts were measured between 240 and 500 nm using the pure solvent as a reference. The concentration of the UV filter was calculated from the determined absorption maxima at 308 nm on the basis of a calibration curve for this substance in ethanol.

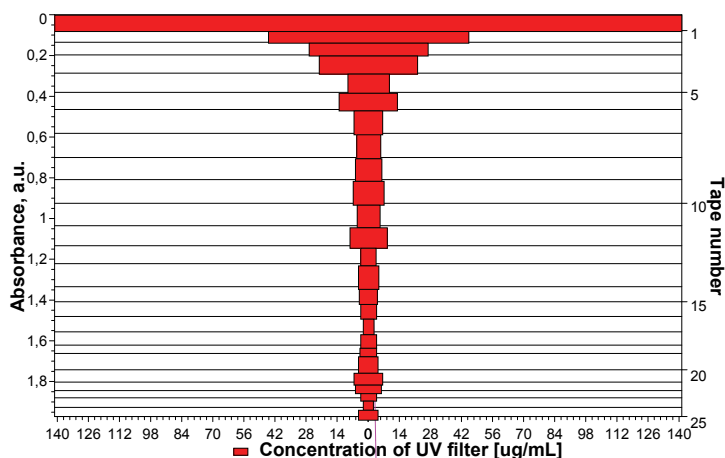


Fig. 4. In-depth distribution of chemical UV filter (utilized in sunscreens), within the porcine stratum corneum, as revealed by the tape stripping technique.

3.2.2 Optical properties in UV range

The dependences of the scattering and absorption coefficients of the stratum corneum on wavelengths within the UV spectral range are shown in Fig. 5. The experimental data (filled squares) were taken from the literature (Cheong *et al.* 1990) and approximated by a linear decay for the scattering coefficient and an an

exponential decay for the absorption coefficient. It is worth mentioning here that both coefficients for the stratum corneum are considerably larger than those corresponding to other skin layers (dermis, epidermis) (van Gemert *et al.* 1989). Absorption is strongly affected by urocanic acid and such amino acids as tryptophan and tyrosin, since they are the main chromophores of the horny layer (Bruls, Slaper *et al.* 1984; Young 1997). The dependence of the transmission on the thickness of the stratum corenum could be described as satisfactory by an exponential function, implying that the Lambert-Beer law is approximately valid (Bruls, Slaper *et al.* 1984).

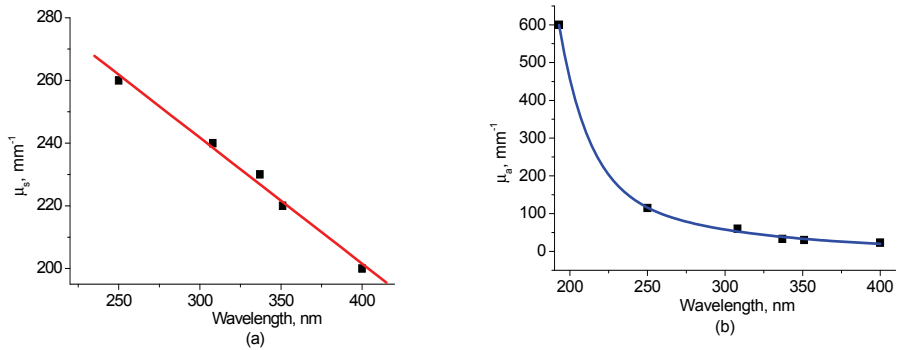


Fig. 5. Scattering (a) and absorption (b) coefficient of stratum corneum (adopted from Cheong *et al.* 1990).

4 Porcine and human skin: comparison

Porcine skin has been used extensively in biomedical and particularly in pharmacological and toxicological research because of similarities of some properties with human skin (Simon & Maibach 2000).

4.1 Penetration studies

The abovementioned properties include permeability; morphology; hair follicle, sweat and sebaceous glands contents. The permeability of different substances (haloprogin, N-acetylcysteine, cortisone, testosterone, caffeine, and butter yellow) contained radioactive labels (^{14}C and ^{35}S) through the whole thickness of skin *in vivo* was studied by detecting penetrated substances in urine 5 days after application. A comparison was made between the dorsal and midlumbar regions of pigs and the ventral forearm of humans (Bartek *et al.* 1972). It was revealed that overall, the skin of a miniature swine had the closest permeability characteristics to that of human skin with this series of compounds.

Jacobi, Toll, Audring *et al.* (2005), investigated *in vivo* the penetration of sodium fluorescein dye on human lips and *in vitro* on a porcine snout, using a dermatological laser scanning microscope; the biopsies were analyzed by laser scanning fluorescence microscopy. The studies revealed the accumulation of sodium fluorescein in the uppermost part of the skin, proving the high efficiency of the barrier function of the stratum corneum. In a number of experiments (Jacobi, Toll, Sterry *et al.* 2005) penetration of the same object – sodium fluorescein – into the stratum corneum and hair follicles of pigs' ears was investigated *in vitro*. In addition, the distribution of the dye from the acceptor fluid (located under epidermis) within the complete tissue was obtained. Both results are similar to those observed *in vitro* on human skin.

4.2 Morphology and thickness

Morphology of a porcine snout and human lips was investigated by histological technique (Jacobi, Toll, Audring *et al.* 2005). It was found that the structure of both organs was quite similar, although the porcine stratum corneum was three-times thicker than a human one (38–88 μm and 13–28 μm , respectively) and the epidermis was 1.5 times thicker (115–198 μm versus 74–148 μm).

The porcine ear skin by comparison to other body areas shows a high degree of similarity to that of human skin (Jacobi, Kaiser *et al.* 2007): the thickness of the horny layer is about 21 μm (6–19 μm for humans), the thickness of the epidermis is about 72 μm (70 μm for human shoulders and 82 μm for buttocks); the density of hair is also quite similar: 20 items were observed on a 1 cm^2 versus 14–32 vellus hairs per cm^2 in humans. The diameters of both porcine hairs (82 μm) and infundibular orifices (200 μm) are larger than those of humans (vellus hairs of 16–18 μm in diameter on most body regions and orifices of 78 μm on forearm and of 66 μm on forehead). Nevertheless, pig ear skin seems to be the most suitable as *in vitro* model for human skin, at least in studies on percutaneous absorption.

4.3 Tape stripping procedure

The tape stripping technique is widely used to reconstruct in-depth penetration profiles of topically applied substances within the stratum corneum *in vivo* (Weigmann *et al.* 1999; Weigmann *et al.* 2001; Jacobi *et al.* 2003; Lindemann, Weigmann *et al.* 2003; Lindemann, Wilken *et al.* 2003). During the procedure, thin strips of stratum corneum are removed one by one from the same skin area. This method is minimally invasive because only dead cells are removed. It is described in detail in numerous publications of Prof. Lademann and colleagues (Weigmann *et al.* 2003; Jacobi, Weigmann *et al.* 2004; Jacobi, Kaiser *et al.* 2005; Weigmann, Jacobi *et al.* 2005; Teichmann *et al.* 2005). After tape application, the area is covered with a piece of paper and 5 there-and-back movements with a roller are made to force the skin to stick to the tape homogeneously. It is therefore essential to keep constant pressure on the skin surface. A tape is removed with one quick movement and fixed onto a frame. A series of up to 100 strips are taken to completely remove the stratum corneum.

In our experiments, we utilized the ear skin of freshly slaughtered German domestic pigs. The ears were used within 0–4 days after delivery. Before treatment they were stored in a fridge at a constant temperature. On the day of experiment, the ears were taken out of the fridge for 1 hour to warm up. They were subsequently carefully washed with running cold water from the tap to remove traces of contamination (sebum, sweat etc.) and then wiped with a paper napkin. The whole ear (or its piece) was fixed with nails on a foam plastic plate wrapped with aluminium foil. In addition to this, hairs were removed from the area under investigation with medical scissors with bent cutting surfaces (to avoid destruction of the skin).

The area chosen for tape stripping was marked with a water-resistant marker. Adhesive 19-mm thick tape Tesa film No. 5529 (Beiersdorf, Germany) was used during the procedure. Plastic frames were utilized as tape holders. Frames with empty and corneocytes-covered tapes were weighted on a precision balance (model BP 211D, Sartorius, Germany) with an accuracy of 0.01 mg before and after stripping to reveal surface density (mass per cm²) of corneocytes attached to the tapes. A 1 min delay was needed in order to allow the balance to come to a steady state. The researcher's hands were covered by gloves and pincers were used during the whole procedure.

4.4 UV/VIS spectroscopy

Spectroscopic measurements were carried out within a wavelength range of 300–1050 nm, utilizing spectrophotometer Lambda 20 (PerkinElmer, Germany) connected to a computer. Transmittance through 1 × 1 cm² tape strip with corneocytes was detected; a tape free of corneocytes was used as reference. The transmittance spectra were plotted in real-time mode on a computer screen. Such spectra can be converted automatically to absorbance spectra by the embedded software, according to the relation $A = \lg(1/T)$, where A means absorbance and T transmittance.

Histograms demonstrating the distribution of absorbance versus strip number for the two marginal wavelengths of the investigated range (300 and 1050 nm) are shown in Fig. 6 (I).

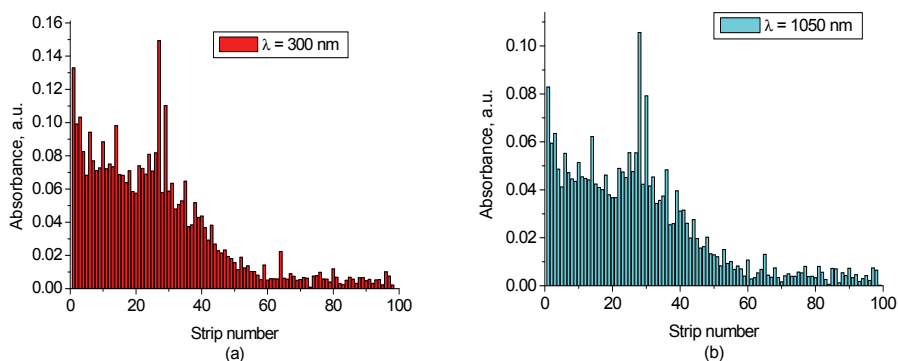


Fig. 6. Absorbance measured separately for each skin strip for 100 strips at 300- (a) and 1050-nm (b) wavelength (I).

Both plots look similar, regardless of the wavelength, although the vertical scales are different, in which absorbance of the light of the shorter wavelength is more pronounced. In fact, corneocytes both absorb and scatter light; the term “pseudoabsorption” might therefore be applied following the earlier published papers (Weigmann *et al.* 1999; Weigmann *et al.* 2001). Usually, absorbance decreases with the increasing strip number. It means that the thickness of cell layers stuck to the tape diminishes. This is caused by a higher degree of cohesion between the corneocytes in deeper cell layers. However, in the picture, one can see features: some strips are out of order (near No. 30). It can be caused by e.g. excessive pressure applied to the roller during the stripping procedure. Such strips are excluded from the further consideration. It is worth mentioning also that contribution of the strips with numbers larger than 60 is considerably smaller than that of other ones.

The cumulative absorbance of cells for four wavelengths (300, 550, 800, and 1050 nm) is represented in Fig. 7 (a). It means that absorbance is summarized consecutively for corneocytes on the first strip, then – on the first two strips, then – on the first three strips etc. until all the strips are taken into account. All four curves coincide within the whole strip number range. The picture also shows distinctly that the contribution of strips No. 60–100 hardly exceeds 10% of total absorbance. Fitting one of these curves (for 300-nm radiation) by an exponential function (red line in the colored version) is illustrated in Fig. 7 (b).

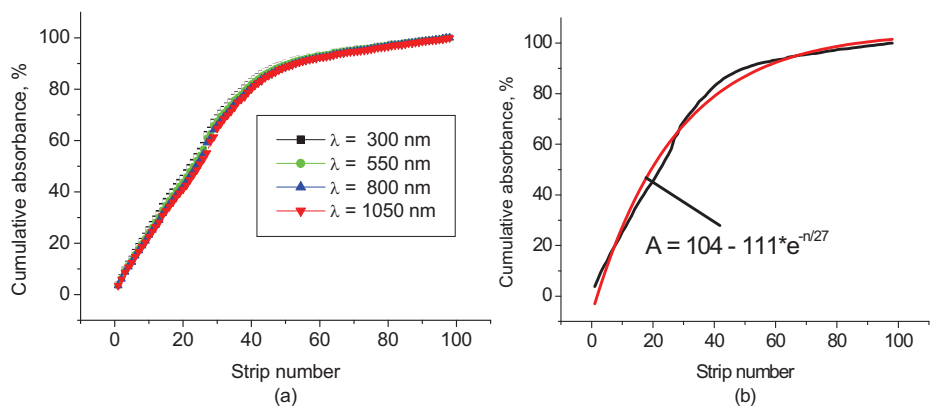


Fig. 7. Cumulative absorbance relative to the strip number for four chosen wavelengths (a) and for 300-nm light approximated by an exponential curve (b, red line in the colored version). This is in good correlation with human skin: $107 - 111 \cdot \exp(-n/21)$ (Jacobi, Weigmann *et al.* 2005).

Comparison between porcine and human skin is satisfactory: for swine $A = 104 - 111 \cdot \exp(-n/27)$ and for humans $A = 107 - 111 \cdot \exp(-n/21)$ (Jacobi, Weigmann *et al.* 2005), where n is a tape strip number.

The removed strips were weighed to ascertain the correlation between absorbance and surface density of corneocytes. The latter was calculated as a ratio of cells mass on the tape and the area covered by them (the width of the tape was constant: 19 mm; the length varied from 39 to 42 mm). A spectroscopic method of estimating cell layer thickness is more convenient and faster than the weighing procedure. However, some residues such as sweat, sebum, and interstitial fluid can affect both the measured weight, from one side (Weigmann *et al.* 2003) and the optical properties of corneocytes (some kind of optical clearing) – from the other. All the sample strips should therefore be carefully examined and those, which do not follow the trend, should be excluded from the further consideration. The linear correlation between absorbance and surface density was found and is shown in Fig. 8 (a). Dependency of the correlation coefficient revealed from four measurements of different samples on wavelength is represented in Fig. 8 (b). Relative error does not exceed 4%.

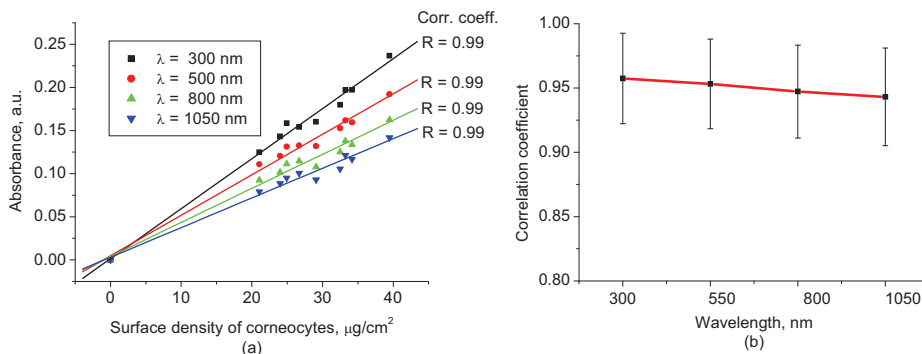


Fig. 8. Relationship between absorbance at different wavelengths and surface density of corneocytes (a) and correlation coefficient calculated from four independent measurements for the same wavelengths (b). Strips disturbed by uneven distribution of cells, sebum, hairs etc. are excluded.

4.5 Visualization of corneocytes

In order to get images of corneocytes, laser scanning fluorescence microscopy was used. The system called Stratum (OptiScan, Australia) was based on Ar⁺ laser emitting light at the wavelength of 488 nm. This radiation is within the absorption band of the dye sodium fluorescein (0.1% water solution) used as visualizing substance. It was applied directly onto skin strips. The fluorescence signal (peak at 590 nm) was collected by an objective lens fixed in a hand-held holder and transferred by a fiber to the photodetector. Such a system was extensively used previously for dermatological purposes, such as studying the accumulation of fluorescent dyes in hair follicles (Otberg *et al.* 2003) and in stratum corneum (Lademann, Richter *et al.* 2003; Jacobi, Waibler *et al.* 2004), *in vivo* determinations of doxorubicin and its metabolites within the skin (Jacobi, Waibler *et al.* 2005), revealing of open and closed follicles spectroscopically (Otberg, Richter, Knuttel *et al.* 2004), *in vivo* imaging of *Malassezia* yeasts on human skin (Meyer *et al.* 2004), efficacy of skin care products (Teichmann *et al.* 2006), evaluation of barrier creams (Rieger *et al.* 2007) and optical characterization of different skin abnormalities, e.g. mycoses, sunburn, psoriasis, basal cell carcinoma (Meyer *et al.* 2006).

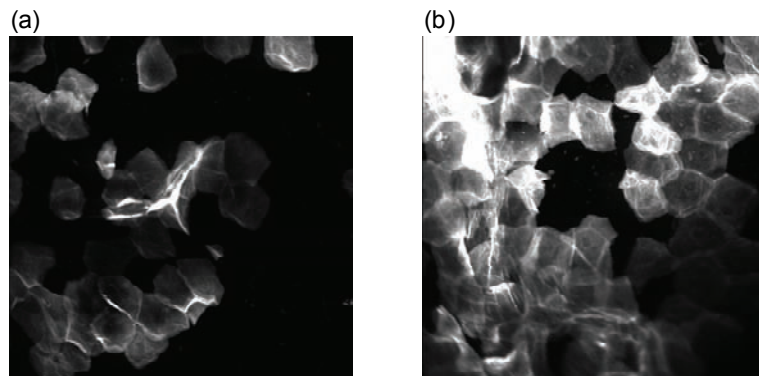


Fig. 9. Images of corneocytes on the 5-th strip: porcine (a) and human (b) cells obtained by laser scanning fluorescent microscope based on Ar⁺ laser source (488 nm). Fluorescent substance sodium fluorescein was used. Picture dimensions are 250 μ m x 250 μ m (l).

Black-and-white images of investigated objects were displayed on a computer screen on a real-time scale. Rotating a small wheel located on the hand-held holder, the length of one of the optical arms was modified, allowing for in-depth scanning.

By analysing images taken from different strips, it was possible to follow in-depth morphology changes of the cells. From Fig. 9 (a) one can estimate also porcine corneocytes sizes: about 30 μm in diameter. Human cells look similar (Fig. 9 (b)) and their dimensions are more or less the same, as can be concluded from the comparison of the two images.

5 UV radiation

5.1 Solar spectrum

The solar spectrum above the atmosphere and at the sea level is represented in Fig. 10 (Gueymard *et al.* 2002). Due to absorption of certain compounds in the atmosphere (ozone O₃, oxygen O₂, carbon dioxide CO₂, water vapour H₂O), the spectrum reaching the Earth surface loses some spectral lines in its different parts.

UV radiation is a part of the solar spectrum occupying a range of 100–400 nm. It is conventionally divided into three sub-ranges (McKinlay & Diffey 1987a): UVC (100–280 nm), UVB (280–315 nm) and UVA (315–400 nm). The former is completely absorbed by the ozone layer of the atmosphere located at a height of 18–40 km above the Earth's surface. The latter two are also attenuated: UVB – about 25 times, UVA – about 2 times, so that both fractions represent 5% of the solar intensity. They reach the atmosphere-ground interface and affect humans. Both types of rays could be harmful if a dose of radiation on the skin is exceeded.

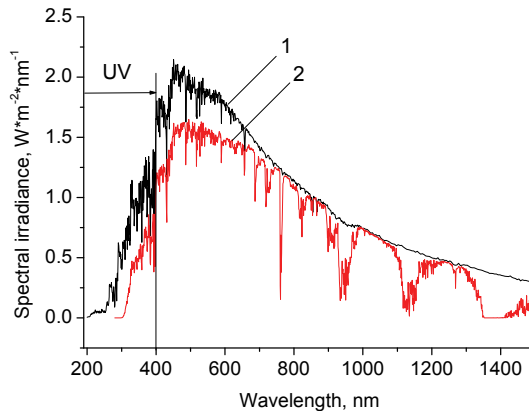


Fig. 10. Solar spectrum above the atmosphere (1) and at the sea level (2) (Gueymard *et al.* 2002).

5.2 Effects on skin

The influence of UV radiation can be divided into two categories: acute and chronic (Diffey 1991). The former includes sunburn and sun tanning as well as production of vitamin D. The chronic effects of these are skin cancer and

photoaging. The UVB fraction is responsible for sunburn and increases the risk of the certain types of skin cancer (basal-cell carcinoma and squamous cell carcinoma) due to direct DNA damage, which is mainly the formation of a thymine-thymine dimer. The UVA fraction causes sun tanning, photoaging, and malignant melanoma by indirect DNA damage (by means of free radical formation). Although malignant melanoma is rare, it is responsible for 75% of all skin-cancer-related deaths. According to investigations, it is found that 92% of all melanoma cases are caused by indirect DNA damage and only 8% of the melanoma is caused by direct DNA damage (Davies *et al.* 2002). Moderate sun tanning can prevent sunburn due to increased production of melanin, which is natural protector against overexposure of human skin to UV radiation because of pronounced absorption within UV spectral range.

5.3 Action spectrum and effective spectrum

The terrestrial solar spectrum contains a pronounced maximum somewhere near 500 nm (green light); the spectral intensity of UV radiation (400 nm and shorter) is considerably lower. Nevertheless, photons of the shortest fraction of the represented spectrum are the most powerful and therefore more dangerous than those of the other spectral regions. Action spectra of the susceptibility of the human skin to erythema (McKinlay & Diffey 1987b) and of generalized DNA damage (Setlow 1974; Setlow 1993) due to UV radiation are shown in Fig. 11.

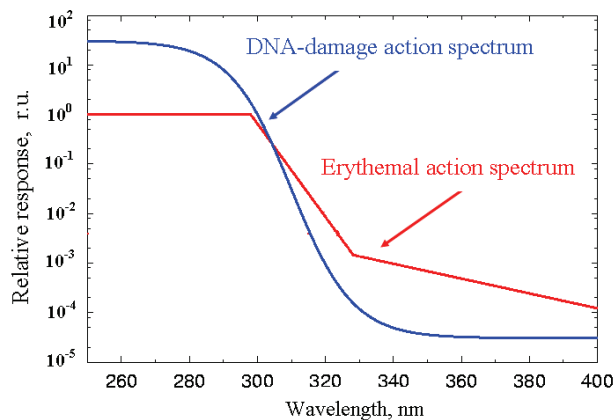


Fig. 11. Erythema and DNA-damage action spectra (McKinlay & Diffey 1987b).

As can be seen from the graph, erythema can more or less indicate the increasing probability of DNA damage, at least for wavelengths shorter than 310 nm. The action spectrum is a parameter that describes the relative effectiveness of energy at different wavelengths in producing a particular biological response. “Biological response” may refer to effects at a molecular level, such as DNA damage, or at a whole organism level, such as plant growth. An action spectrum is used as a “weighting factor” for the UV spectrum to find the actual biologically effective dose for a given effect. Multiplying the plots from Figs. 10 and 11 (erythema action spectrum), one can evaluate the effective spectrum taking into account the spectral intensity of wavelengths within the original solar spectrum (Fig. 10). The result of such a procedure is shown in Fig. 12 (IV). One can conclude from this plot that erythema dangerous zone is 305–320 nm (mostly UVB range).

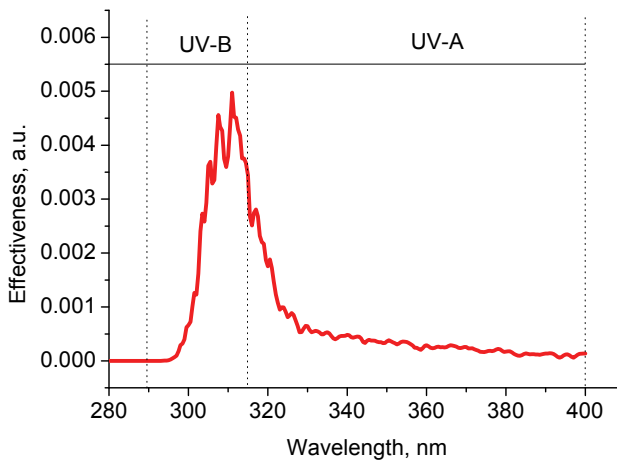


Fig. 12. Effective spectrum of solar radiation within UV spectral range (IV).

6 Nanoparticles of titanium dioxide

In order to improve the UV protective function of the stratum corneum, chemical and physical compounds are added to sunscreens (Edlich *et al.* 2004; Jacobi, Weigmann *et al.* 2004). The former are absorbing organic chemical substances while the latter are nanoparticles of titanium dioxide (TiO_2) and zinc oxide (ZnO) (Innes *et al.* 2002) which both absorb and scatter UV light. Recently, silicon (Si) nanoparticles were suggested for use in sunscreens (Rybalovsky *et al.* 2006).

TiO_2 nanoparticles are extensively used nowadays also in cosmetics, paints, air and water waste purification (Diebold 2003). Among the three existing crystal modifications of TiO_2 (anatase, rutile and brookite), rutile and anatase are used widely. Their crystal structures are represented in Fig. 13.

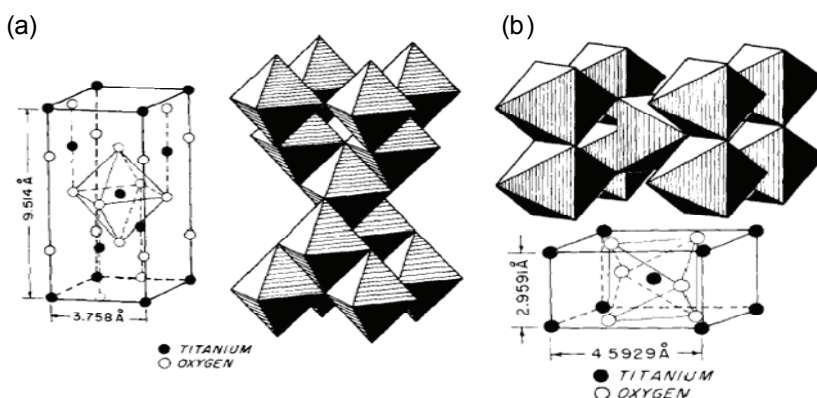


Fig. 13. Crystal structures of anatase (a) and rutile (b) (www.millenniumchem.com).

Energy band gaps in anatase and rutile are 3.2 and 3.0 eV, respectively; such gaps correspond to the wavelengths of 388 and 414 nm. Data about the photoactivity (phototoxicity) of different crystal forms are contradictory: some authors report that anatase is the most photoactive, if irradiated by UV light (Cao *et al.* 1999, Kakinoki *et al.* 2004), while the others claim that either rutile form (Watson *et al.* 2003) or mixture of rutile and anatase (Bakarjieva *et al.* 2005) are the most active. As indicated in the cited publications, photoactivity strongly depends on relative humidity, preparation temperature, production process, particle size, as well as on dopants (Zhang *et al.* 1998), coating and correlates with the reflectance spectra (Vorontsov *et al.* 2001). The photocatalytic activity of titanium dioxide, resulting in

free radical generation in skin, is a negative factor, which is essentially suppressed by coating the particles with silica (SiO_2), dimethicone or alumina (Al_2O_3) (Warner *et al.* 1997; Lademann *et al.* 2000). Both anatase and rutile particles used in sunscreens oxidize DNA and RNA *in vitro* and in human cell culture (Dunford *et al.* 1997; Hidaka *et al.* 1997) under UV irradiation. However, it is important to know, whether the amount of radicals generated by the particles on the skin exceeds that produced by the skin itself.

Nanoparticles tend to form aggregates and agglomerates of 100–200 nm in size, worsening their protecting properties in the UVB range and shifting the pronounced attenuation to the longer wavelength UVA and visible regions of the solar spectrum. The typical organization of anatase particles of different diameters (25 and 400 nm) are shown in Fig. 14. Nevertheless, novel manufacturing technologies, e.g., mechanochemical processing (MCP™) enable the production of nanopowders without such disadvantages and with a narrow size distribution (25 ± 4 nm) which can be successfully used in sunscreens (Innes *et al.* 2002). The usual size distribution of TiO_2 particles is 15–20% from the mean value (Ahonen *et al.* 2001).

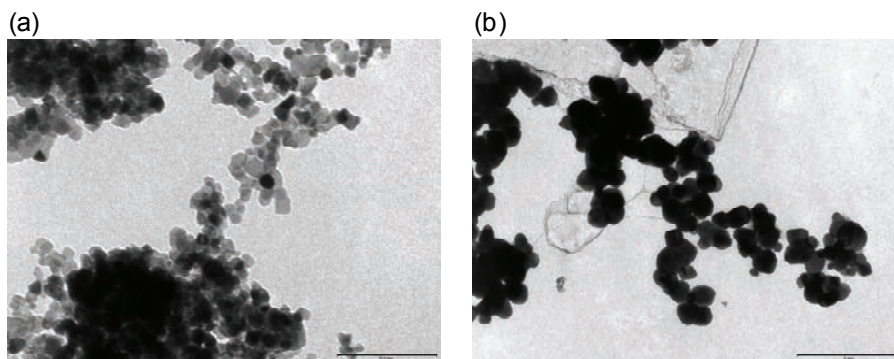


Fig. 14. TEM photos of 25- (a) and 400-nm (b) nanoparticles of titanium dioxide. Magnification: x110 (a) and x22 (b). Scale: bar corresponds either to 0.2 μm (a) or 1 μm (b).

7 Free radical generation under UV irradiation

7.1 Free radicals

Free radicals are molecules with an unpaired electron on the external orbital and of high chemical reactivity. All radicals existing in the human organism can be divided into two kinds: natural and alien. The former are those which are inherently produced in the organism during chemical reactions: radical oxygen species (ROS) such as superoxide (O_2^-), singlet oxygen (1O_2), hydroxyl radical (OH); as well as nitric oxide (NO) etc. They play an important role as regulatory mediators in signalling processes such as regulation of vascular tone, monitoring of oxygen tension in the control of ventilation and erythropoietin production and signal transduction from membrane receptors in various physiological processes (Darr & Fridovich 1994; Dröge 2002). Under normal conditions, the amount of free radicals is balanced by enzymes and antioxidants. An excessive increase in ROS production occurs in, for example, the pathogenesis of cancer, diabetes mellitus, atherosclerosis, neurodegenerative diseases, rheumatoid arthritis, ischemia/reperfusion injury (Dröge 2002). The alien free radicals appear as a consequence of the effect of ionizing radiation, UV light, xenobiotics, etc. on human tissue and are harmful.

7.2 EPR technique

The study of free radicals can be carried out by direct and indirect methods. The former implement the effects of either electron paramagnetic resonance (EPR) or chemoluminescence. The latter include investigations of the end products of the reactions with free radicals involved or application of inhibitors. The EPR (also called ESR – electron spin resonance) technique is based on the absorption of microwave radiation by an unpaired electron of a molecule located in a magnetic field.

Direct detection of short-lived free radicals by the EPR method is possible only at quite low temperature (77 K, liquid nitrogen), owing to their sufficient steady-state concentrations only under such conditions (Fuchs *et al.* 2001). In order to achieve suitable concentrations at room temperature, spin traps and spin markers are used (e.g., PCA, DPPH, Tempol, TEMPO, DMPO, 4-POBN). Spin traps are molecules, which bind to short-lived free radicals and form detectable stable forms

of radicals (spin adducts). Spin markers are stabilized radicals contributing to the EPR signal; however, being in contact with short-lived free radicals stabilized radicals lose or add an electron and become undetectable. The decrease in the EPR signal in this case quantifies the free radicals under investigation. The EPR methodology is a useful tool for the non-invasive *in vivo* measurements of skin barrier function, drug/skin interaction and cutaneous oxygen tension (Fuchs *et al.* 2001).

Skin is a tissue protecting deeper located organs from various hazards of the environment, such as chemical, biological and physical, in particular, from UV light. Excessive doses of UV radiation can cause direct or indirect (via formation of free radicals) DNA damage leading to carcinogenesis (Ananthaswamy & Pierceall 1990). Skin is a suitable object for EPR investigations because of its surface location and relatively small thickness. Using the microwave radiation of 1–10 GHz, which penetrates as deep as 1–35 mm into the skin, it is possible to monitor the penetration of spin traps and spin markers inside the skin (Herrling, Fuchs *et al.* 2002; Meinke *et al.* 2008) and the in-depth appearance of generated radicals by means of EPR imaging (Herrling *et al.* 2005). According to investigations, UV-induced radicals include ROS and lipid radicals (Nishi *et al.* 1991; Ogura *et al.* 1991; Herrling *et al.* 2003) as well as melanin radicals (Collins *et al.* 1995). As shown by experiments with human skin *in vivo* (Herrling, Zastrow *et al.* 2002), the UVA part of the UV spectrum (290–320 nm) is mainly responsible for the generation of free radicals (80–90% of total amount) because of higher penetration depth, in contrast to UVB light (320–400 nm) which contributes to radical generation only in the epidermis (up to a depth of 200 μm).

7.3 Experiments with TiO₂ nanoparticles

Two types of samples were used in the experiments: placebo (sunscreen o/w emulsion without any filters, Creme Sante soleil SPF 8 F148-006 (RoC, France)) with coated TiO₂ nanoparticles embedded. The samples were applied either onto glass slides or onto porcine skin *in vitro*. TEM images of the particles used are depicted in Fig. 14. The surface density of the substance was 2 mg cm⁻² corresponding to the recommendations of COLIPA (COLIPA 1994) for sunscreen applications. The placebo was weighed on a precise balance BP 211D (Sartorius, Germany) with an accuracy of 0.1 mg using a syringe. One type of spin marker, PCA (Sigma-Aldrich Chemie, Germany), was used to detect short-lived free radicals emerging under UV irradiation. PCA was dissolved from powder in a

water-ethanol (1:1) solution at a concentration of 10 mM. It was chosen from other available spin markers owing to its satisfactory stability for our applications: after a 3 minute-long UV irradiation, the EPR signal decrease was about 1% and after an 18 minute-long irradiation – only 6% (Haag 2007). Additionally, in porcine skin there are low amounts of antioxidants, thus prolonging the existence on PCA. As a source of UV radiation (280–400 nm) a device TH-1E (Cosmedico Medizintechnik, Germany) was used. The radiation intensity was 4.3 mW cm^{-2} measured by the powermeter HBM-1 (Hydrosun Medizintechnik, Germany), which corresponds to the solar UV intensity (4.6 mW cm^{-2}). The EPR system LBM MT 03 (Magnetech, Germany) operating in L-band (1–1.5 GHz) of 46 mT magnetic field strength with magnetic field modulation (frequency – 100 kHz, magnitude – 0.15 mT) was used for detecting the EPR signal. The generated short-lived radicals react with the pyrrolidine nitroxide PCA, which is thereby reduced to the corresponding hydroxylamine. PCA loses its free electron and the signal intensity in the EPR signal decreases correspondingly.

7.3.1 Raman spectroscopy

The Raman spectroscopy system (LMTB, Germany) (Darvin *et al.* 2005; Darvin *et al.* 2006; Darwin *et al.* 2006) was based on a CW Ar^+ laser operating at the wavelength of 514.5 nm (power 9 mW).

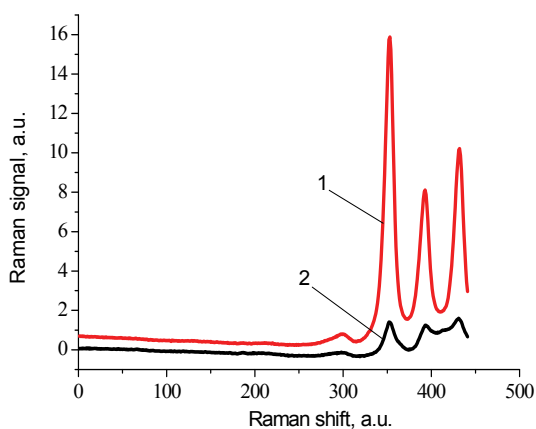


Fig. 15. Signal of Raman scattering from powder titanium dioxide nanoparticles with diameters of 400 nm (1) and 25 nm (2).

In order to reveal the crystal form of the used titanium dioxide particles, Raman spectra of the powders of particles of two sizes were measured. The obtained spectra are presented in Fig. 15. The signal produced by 25-nm particles is much smaller than the signal produced by 400-nm ones, owing to features of particles-light interaction. Three obvious peaks appear in the graph. These indicate, according to Jackson (1998), that the crystal form of the particles under investigation is anatase.

7.3.2 Mie calculations

For Mie calculations, MieTab 7.23 software (<http://amiller.nmsu.edu/mietab.html>) was used. As input parameters, the radiation wavelength, refractive indices of the particles and the surrounding medium, as well as particle sizes were required.

The Mie theory was used to describe the interaction between the particles and UV radiation. The spectrum of the UV light source is depicted in Fig. 16. For the calculations, two wavelengths were chosen: 310 nm and 335 nm. The first one was chosen because it was close to the maximum of the source spectrum and corresponded to the maximum of the product of the solar spectral irradiance over wavelength with the erythemal action spectrum (IV). The second one was taken for comparison.

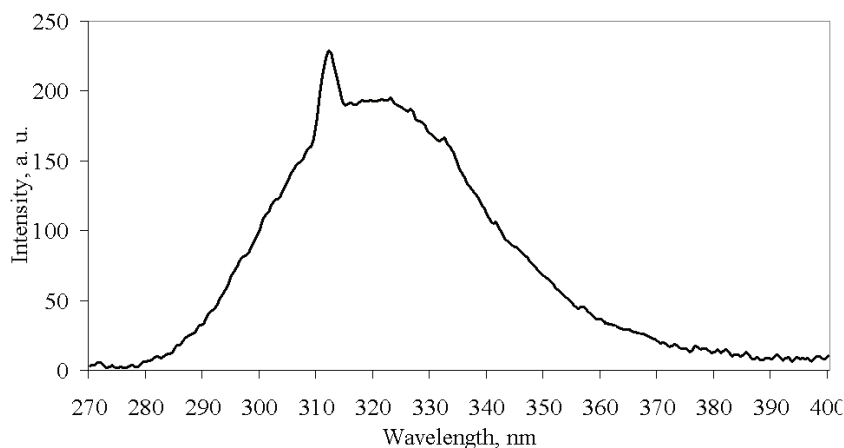


Fig. 16. Spectrum of the UV lamp used in the experiment.

Titanium dioxide is a birefringent crystal, with different refractive indices for light polarized perpendicular or parallel to the optic axis. In the “average index”

approximation, the particles are supposed to be isotropic, with real and imaginary parts of the refractive index equal to $n_p = (2n_o + n_e)/3$ and $k_p = (2k_o + k_e)/3$, where n_o and k_o (n_e and k_e) are the ordinary (extraordinary) real and imaginary parts of the refractive index, respectively (Palmer *et al.* 1989). For the 310-nm and 335-nm UV radiation these constants taken from (Jellison *et al.* 2003) result in: $n_p - i k_p = 3.48 - i 0.83$ (for 310 nm) and $n_p - i k_p = 3.37 - i 0.25$ (for 335 nm). The refractive index of the surrounding medium (placebo) was 1.4, the diameters of the particles were considered to be 2–200 nm with 2-nm steps. The result of the calculation is shown in Fig. 17. Absorption efficiency factor Q_a is the ratio of the absorption and the geometrical cross-sections of a particle. The value (Q_a/d) , where d is a particle diameter, is proportional to the absorption coefficient of a particle suspension (V, VI, Popov *et al.* 2006b) and therefore takes into account the presence of other particles of the same type in the sample.

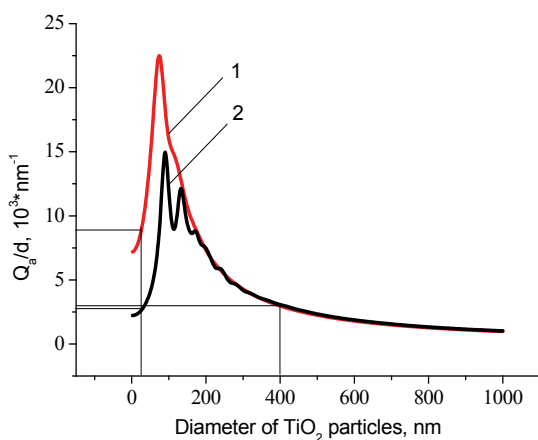


Fig. 17. Relative absorption efficiency factor referred to the particle diameter (Q_{abs}/d) for 310- (1) and 335-nm (2) UV radiation calculated according to the Mie theory, maxima of the curves correspond to the particle diameters of 74 and 90 nm.

7.3.3 Experiments on glass slides

The glass slides had the following dimensions: width – 2.5 cm, length – 5 cm, thickness – 2 mm. There were three types of prepared slide samples (5 couples of samples of each type): 1) placebo with small (25 nm in size) particles, 2) placebo with large (400 nm) particles, 3) placebo only. The slides were covered

homogeneously with a mixture of the corresponding substances (2 mg cm^{-2}) and PCA ($50 \text{ }\mu\text{l}$). In each couple, one sample was irradiated with the UV lamp (25-nm particles – for 1 min, 400-nm ones and placebo only – for 2 min); the other was used for control (was not irradiated). The samples were put into the EPR system and measured before and after the irradiation. The signals were displayed in real time on the computer screen in the software environment supplied with the system. They were stored as files and then analyzed.

Fig. 18 shows the mean values with standard deviations of the results obtained from 5 samples on glass with or without particles (Popov *et al.* 2008). Standard deviations vary between 0.02 and 0.24 for non-irradiated samples and 0.10 and 0.26 for the irradiated samples.

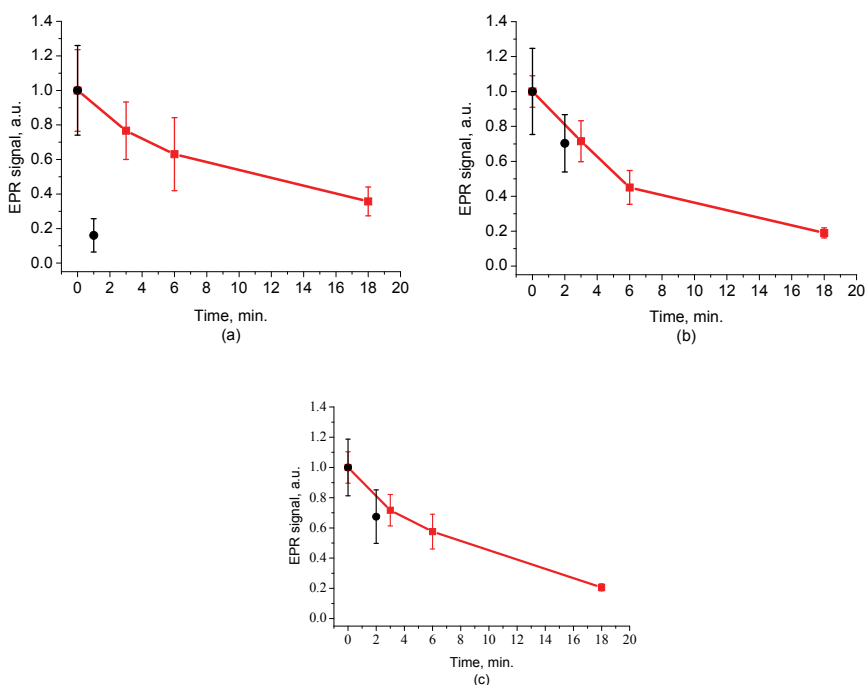


Fig. 18. Temporal dependences of amplitudes of the EPR signals obtained from the samples on glass: placebo with 25-nm particles (a), placebo with 400-nm (b) particles and placebo without particles (c) UV-irradiated during 1 min (a) or 2 min (b, c) (●) and not irradiated (■). Zero-time corresponds to the beginning of UV irradiation (for the irradiated samples) (Popov *et al.* 2008).

Dependences of the EPR signal amplitudes on time for the irradiated and non-irradiated samples are depicted. Statistically, there is no effect of UV radiation in the presence of large particles and placebo without particles. However, the effect is distinctly seen in the case of small particles, although they were irradiated for a shorter time (1 min). This phenomenon can be explained in the framework of the Mie theory. Considering that Fig. 17 represents the absorption efficiency curves for 310-nm and 335-nm radiation, we can conclude that 25-nm particles absorb UV light much more efficiently than the 400-nm ones for $\lambda = 310$ nm or at the same level for $\lambda = 335$ nm at the same volume concentrations. It is known that the particles tend to form aggregates and agglomerates, although ultrasonic stirring was used during the process of embedding particles into the placebo. The formation of the above-mentioned structures causes an increase in the average size of particles leading to the increased absorption efficacy of the 25-nm particles and decreasing that of the 400-nm particles. Greater absorption means more active production of free short-lived radicals. The curve corresponding to the non-irradiated large particles looks very similar to that of placebo and different from that of small particles.

7.3.4 Experiments on porcine skin in vitro

The ears of domestic pigs were delivered from a nearby farm (Gut Hesterberg, Germany) on the day following the slaughter. Before the experiments, the ears were washed with cold running water and gently wiped with paper napkins. All hairs on surfaces of the ears were completely removed with medical scissors with curved edges to avoid injuring the skin. Then Tesa adhesive tape (Beiersdorf, Germany) was used for tape stripping according to (Weigmann *et al.* 1999). 20 tape strips were taken from the same area to remove the stratum corneum in part. Corresponding to (I), with this number of strips about 50% of stratum corneum was removed. A roller was used to press the tape to the skin. This procedure was required to ease the penetration of the PCA into the skin (Meinke *et al.* 2008). The PCA served as a marker for revealing the production of free radicals. In the investigation of free radicals with the EPR technique, the deeper the PCA penetrated, the higher the amount of skin volume was involved.

The surface of each porcine ear area, 5×14 cm² in size, was marked with a permanent marker. The areas were divided into pairs of small areas of 2.5×4 cm² or 2.5×3 cm². One area in the pair was used immediately after the preparation procedure was completed; the other area was used 25–30 min after the application

of substances. The borders of all the areas were covered with a colour glue to build barriers between neighbouring areas. As with the experiments that applied particles onto glass slides, three different substances were investigated: placebo with 25-nm particles, placebo with 400-nm particles and placebo without particles. The PCA was added to all substances (100 μl per each small area). The substances were topically applied onto the skin, with a surface density of 2 mg cm^{-2} . During the application of the corresponding (according to the area) amount of the substances the skin was massaged with a massage device (Petra PC 60, Petra-electric, Germany) covered with a latex glove finger saturated in advance with the substance. From each small area, two punch biopsies were taken with a round-edged sharp cutter: one was later irradiated with the UV lamp (stratum corneum side); the other was used for control. The diameter of the skin samples was 12 mm; the thickness was 2 mm (all skin layers from the surface to the cartilage in the middle of the ear). The biopsies were removed from the ear using a scalpel and pincers and were fixed onto a glass slide using acryl glue. Certain samples were subsequently irradiated by UV light for 3 min. The irradiated samples were measured in the EPR system before, immediately after and 15 min after the irradiation. Those serving as controls were measured at 0, 3, 7, 10, 15 min (zero time corresponds to the start-time point of sample irradiation). Four to six samples were used for each measurement in order to collect statistical data.

One group of skin samples was irradiated immediately after preparation, the other – with a 25–30 minute-long delay. The results of the measurements of the first group with standard deviations are presented in Fig. 19. Standard deviations vary between 0.04 and 0.25 for non-irradiated samples and 0.08 and 0.30 for the irradiated samples. Even with statistical errors taken into account, the effect of UV irradiation is clearly seen in all cases (the points corresponding to such samples are located lower than those of non-irradiated ones), the magnitude of the effect is almost the same for the samples with the particles in placebo, with placebo only and for the skin samples without placebo and particles. This means that the amount of short-lived free radicals appearing under UV irradiation are comparable and do not depend on the presence of the particles on the skin surface. In other words, the contribution of skin to free-radical generation under UV irradiation exceeds that of the particles.

The effect of the penetration time (0 min versus 25–30 min) of the substances before UV irradiation is depicted in Fig. 20. There is no significant difference; it should be mentioned, however, that in the samples corresponding to the large particles (Fig. 20 (b)) as well as to placebo (Fig. 20 (c)) and to skin without

placebo and particles (Fig. 20 (d)), the lines connecting the average values and relative to measurements without any delay are located above the lines corresponding to the delayed experiments. However, the situation is the reverse for the samples with small particles (Fig. 20 (a)).

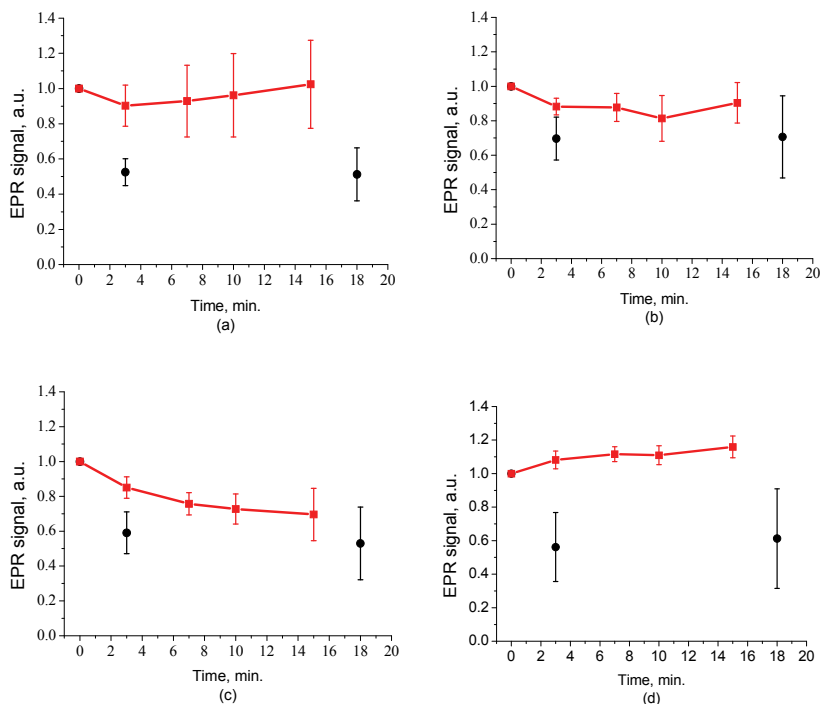


Fig. 19. Temporal dependences of amplitudes of the EPR signals obtained from the samples on porcine skin *in vitro*, measured without delay: placebo with 25-nm (a) or 400-nm (b) particles, placebo without particles (c) and skin without placebo and particles (d) UV-irradiated during 3 min (●) and not irradiated (■). For averaging, 4 skin samples with placebo and each type of the particles, 6 skin samples with placebo only and 6 skin samples without placebo and particles were measured. Zero-time corresponds to the beginning of UV irradiation (for the irradiated samples).

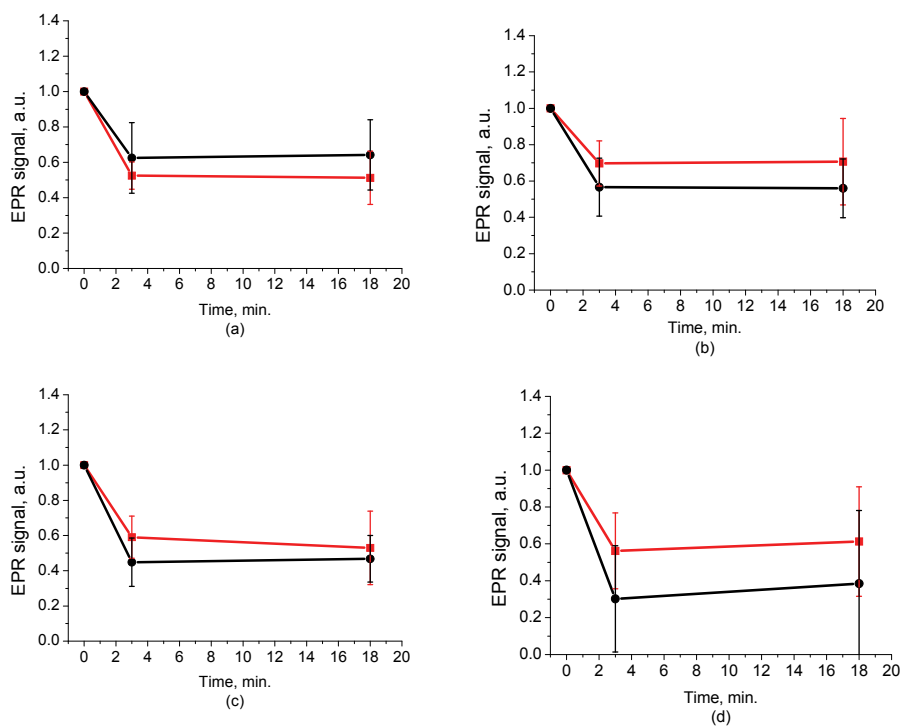


Fig. 20. Comparison of time-dependent amplitudes of the EPR signals after 3 min-long UV irradiation of the skin samples immediately after preparation (■) and 25–30 min later (●): placebo with 25-nm (a) or 400-nm particles (b), placebo without particles (c) and skin without placebo and particles (d). For averaging, 4 skin samples with placebo and each type of the particles, 6 skin samples with placebo only and 6 skin samples without placebo and particles were measured. Zero-time corresponds to the beginning of UV irradiation (for the irradiated samples).

8 UV protection by nanoparticles

8.1 Multiple application of sunscreens on skin: location of particles

The experiment employed the previously-described tape stripping technique (Weigmann *et al.* 2001). The study was performed with 6 healthy volunteers with skin types II and III. An emulsion containing coated titanium dioxide particles (mean diameter 100 nm) was studied, and 2 mg cm^{-2} of this preparation, according to the COLIPA standard (COLIPA 1994), were applied on the flexor forearm. A skin area of $10 \times 8 \text{ cm}^2$ was marked with a permanent marker. 160 mg of the selected emulsion was applied with a syringe and distributed homogenously with a gloved finger. The procedure is illustrated by Fig. 21 (Lademann, Weigmann *et al.* 2005).

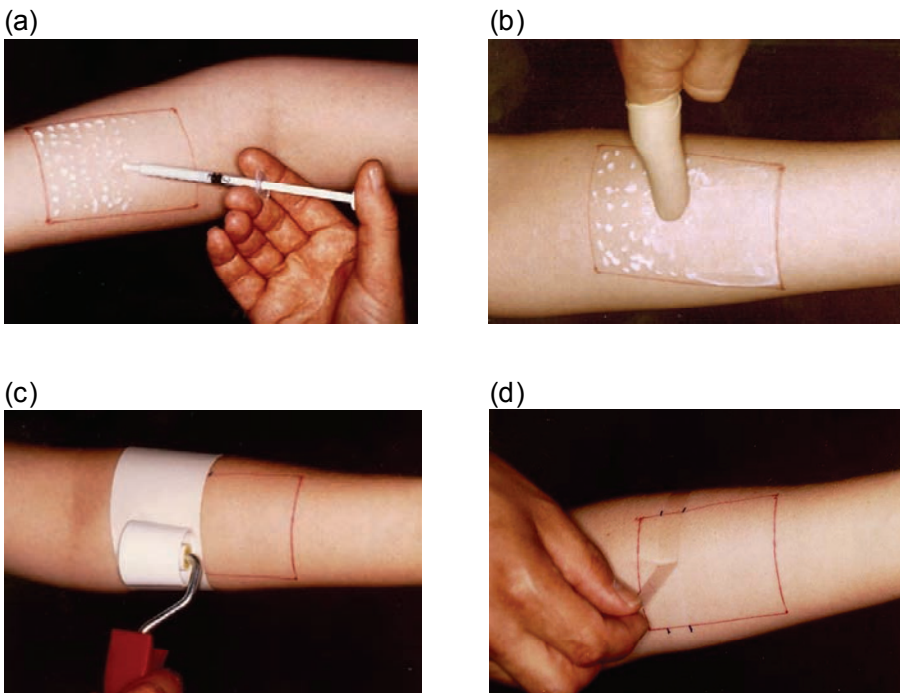


Fig. 21. Application of a sunscreen and tape stripping: application of the emulsion (a), homogeneous distribution with a saturated glove finger (b), pressing of the tape by a roller (c), removing of the adhesive tape (d) (Lademann, Weigmann *et al.* 2005).

After application of the emulsion, the volunteers rested for 1 h, without sweating and without covering the test area with textiles. The model sunscreen with titanium dioxide was administered 5 times over a period of 4 days. The volunteers were allowed to wash the treated skin area and wear any clothes as they would on the beach. The tape stripping started on the fourth day 1 h after application. Such a long period is caused by requirements of dermatologists, when sunscreens are applied before every exposure to the sun, and reapplied frequently and liberally, at least every two hours, as long as staying in the sun, and especially after swimming. This is needed for a more homogeneous, superficial distribution of administered particles. As shown (Lademann, Rudolph *et al.* 2004), the homogeneous distribution can increase effectiveness of sunscreens by a factor of 10 in terms of SPF (sun protection factor), and inversely, an uneven distribution of the applied sunscreens decreases SPF and leads to necessity of use the step model of the treated skin (Ferrero *et al.* 1999).

Thin strips of stratum corneum (about 1- μm -thick each) were removed one by one using Tesa adhesive tape. The penetration profile was obtained by analyzing the amount of the stratum corneum (amount of corneocytes) and that of TiO_2 removed with each tape strip. The thickness of the skin strip relative to the whole thickness of the horny layer was determined spectroscopically (Jacobi *et al.* 2003; Weigmann *et al.* 2003). Due to presence of particles NIR light was used for this purpose (Popov *et al.* 2006a). The surface concentration of the particles in each strip was estimated by X-ray fluorescent measurements (Lademann *et al.* 1999), which yielded about $14 \mu\text{g cm}^{-2}$ in the first strip and almost zero in the strip taken from the depth of $15 \mu\text{m}$. Most of the particles were located within the depth range of 0–3 μm . The results of the procedure are shown in Fig. 22 (VI).

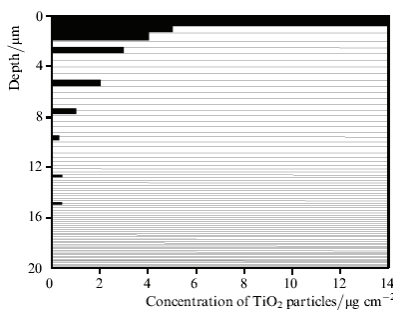


Fig. 22. Experimental determination of TiO_2 particles in-depth distribution within the stratum corneum, obtained by the tape-stripping technique (VI).

Evaluation of the volume concentration of TiO₂ particles C [%, if multiplied by 100] in the uppermost strip (see Fig. 22) can be performed as follows:

$$C = \frac{N \cdot V_0}{V} = \frac{M}{\rho_0 \cdot V_0} \cdot \frac{V_0}{V} = \frac{M}{\rho_0 \cdot V}, \quad (1)$$

where N is the number of TiO₂ particles with volume V_0 and density ρ_0 each, within a strip of volume V . The total mass of all the TiO₂ particles inside the strip is M . The volume V equals to the strip thickness (in our case 0.75 μm) multiplied by the surface area (1 cm^2). As it can be deduced from Fig. 22, mass M equals to 14 μg (because the area is 1 cm^2). Density of TiO₂ (rutile form) ρ_0 is 4 g cm^{-3} . Therefore, it can be calculated that the volume concentration of TiO₂ particles within the uppermost strip is about 5%. In deeper parts of the horny layer the skin contains considerably fewer particles.

8.2 Mie calculations: cross-sections and anisotropy factors

Optical parameters, such as scattering and absorption coefficients (μ_s and μ_a respectively) for a medium partially filled with TiO₂ (or Si) particles, are needed as input data for the Monte Carlo simulations. They can be expressed using scattering σ_s and absorption σ_a cross-sections of a particle. These cross-sections can be either smaller or larger than the geometrical cross-section of a particle because they are a measure of interaction (scattering and absorption) between a photon and a particle. Thus, using the same notations as in the equation (1) we find that

$$\mu_s = \frac{N \cdot \sigma_s}{V} = \frac{C}{V_0} \cdot Q_s \cdot \frac{\pi \cdot d^2}{4} = C \cdot Q_s \cdot \frac{\pi \cdot d^2 / 4}{\pi \cdot d^3 / 6} = 1.5 \cdot \frac{Q_s \cdot C}{d}, \quad (2)$$

$$\mu_a = \frac{N \cdot \sigma_a}{V} = \frac{C}{V_0} \cdot Q_a \cdot \frac{\pi \cdot d^2}{4} = C \cdot Q_a \cdot \frac{\pi \cdot d^2 / 4}{\pi \cdot d^3 / 6} = 1.5 \cdot \frac{Q_a \cdot C}{d}, \quad (3)$$

here $Q_s = \sigma_s / \sigma_g$ and $Q_a = \sigma_a / \sigma_g$ are relative (dimensionless) light scattering and absorption efficiency factors respectively, and $\sigma_g = \pi d^2 / 4$ is the geometrical cross-section of the particle, d is the particle diameter (100 nm in the experiment), C is volume concentration of particles. The efficiency factors Q_s and Q_a were determined using the Mie scattering theory with the help of MieTab 7.23 software. As reported in Shao & Schlossmann (1999), particles 35–200 nm in diameter are of spherical shape. Even for prolate pigment TiO₂ particles with the aspect ratio of about 1.5 the spherical approximation is acceptable (McNeil & French 2000). Real

$Re(n_p)$ and imaginary $Im(n_p)$ parts of the refractive index of TiO₂ and Si particles for the light with the wavelength λ required as input data for this software are represented in Table 1 (Palik 1985). The sum of the two values Q_s and Q_a is called the relative light extinction efficiency factor, Q_{ext} .

Table 1. Real and imaginary parts of refractive indices of TiO₂ (rutile form) and Si for 310- and 400-nm UV light (Palik 1985).

λ , nm	$Re(n_p) - i*Im(n_p)$	
	TiO ₂	Si
310	3.56 - i*1.72	5.01 - i*3.59
400	3.3 - i*0.008	5.57 - i*0.387

The greater the extinction efficiency factor, the higher the attenuation (absorption and scattering) of the radiation transmitted through a sample. However, there is one more parameter of particles-light interaction characterizing light propagation inside a medium; namely, the average cosine of scattering (scattering anisotropy factor), $g = \langle \cos \theta \rangle$. This varies within the interval $[-1, 1]$. Unity is related to the fully forward scattering, negative unity – to the fully backward scattering, while zero value corresponds to isotropic or symmetrical scattering. Assuming the refractive index of the horny layer $n_m = 1.53$ (Tuchin 2000), we calculated the relative scattering, absorption, and extinction efficiency factor Q_s , Q_a , and Q_{ext} respectively, as well as g and constructed a quantity $[Q_a + Q_s*(1 - g)]/d$ for the 310- and 400-nm radiation for the diameters of TiO₂ (and Si) particles ranging from 35 to 200 nm with a step of 2 nm. Such a quantity satisfactorily predicts the most attenuating particle sizes (VI, Popov *et al.* 2007). The results of the calculations are depicted in Fig. 23.

In both parts of the figure the curves corresponding to silicon have more pronounced peaks than those corresponding to titanium dioxide. It means that for the diameters of particles corresponding to the maxima, silicon better attenuates the UV light of the indicated wavelengths. The positions of the maxima are at 56 and 60 nm for Si and TiO₂ particles, respectively, for the 310-nm radiation. For the 400-nm light the maxima are located at 70 (for Si) and 126 (for TiO₂) nm. As can be concluded from the plots, silicon nanoparticles are better protectors almost within the whole range of the considered particles sizes. The most drastic difference between Si and TiO₂ curves is for the wavelength of 400 nm. The Si peak is shifted to the smaller diameters and is much larger than the TiO₂ peaks.

This differs from the 310-nm curves, for which the difference of maxima is not so large and the maxima are located rather close to each other.

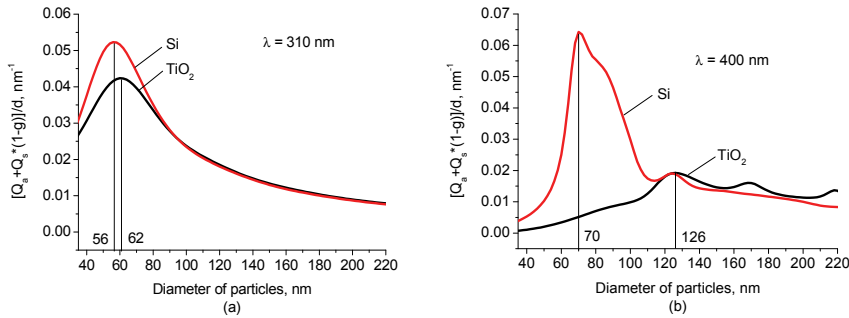


Fig. 23. Dependences of quantity $[Q_a + Q_s \cdot (1 - g)]/d$ on particle diameter for TiO_2 and Si nanoparticles for 310- (a) and 400-nm (b) light.

8.3 Monte Carlo simulations

8.3.1 Model of stratum corneum with particles

As known, the skin surface is not plane (Jacobi, Chen *et al.* 2004): furrows and wrinkles (known as ‘sulci’) are located on its surface and represent a reservoir for topically applied substances. After application of a sunscreen, nanoparticles are accumulated in such structures. This causes uneven distribution of them over the skin surface. Nevertheless, it should be taken into consideration that sulci represent only 10% of the skin surface structure (age of the volunteers: up to 45 years), so most of the skin surface can be approximated as flat surface. Additionally, the area covered by hair follicles is much smaller than the rest of the skin surface (Otberg, Richter, Schaefer *et al.* 2004) because of their small surface density. So it is reasonable for sunscreen protection to take into consideration only skin surface free from follicles. Moreover, the content of TiO_2 particles (if applied) in such follicles is rather low (less than 1% of applied) as experimentally shown (Lademann *et al.* 1999), because the horny layer serves as a barrier. In our experiments the sunscreen with the particles was applied several times during the four days, resulting in a more homogeneous distribution than if administered only once. Taking into account the above mentioned reasons, a plane-layer model (not a step model, as for

uneven distribution of sunscreen (Ferrero *et al* 1999)) of the stratum corneum treated with a sunscreen was developed.

The Monte Carlo method implemented in a developed computer 3D code using Delphi[®] software environment, was applied to simulate the propagation of UV light within the stratum corneum with embedded TiO₂ (or Si) particles (II, III, Popov, Priezzhev *et al.* 2005). Fig. 24 illustrates the geometry of the sample model. Incident light is directed perpendicularly to the air-skin interface. The collimated incidence is modelled instead of diffuse light, which perhaps would be more relevant for a sun-bather (because of curvature of body parts and if some overcast takes place) due to the following reasons.

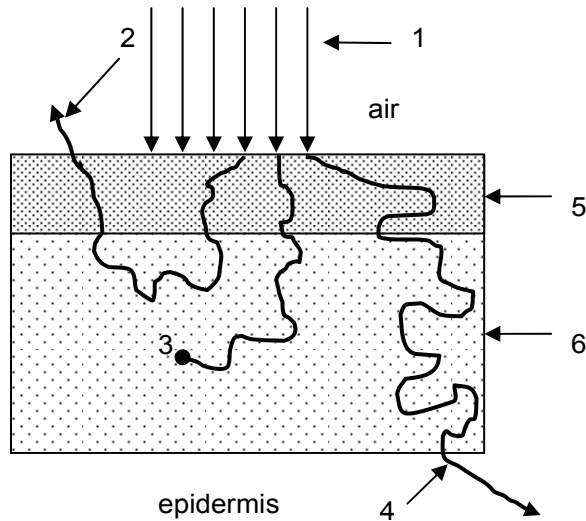


Fig. 24. Model of the stratum corneum partially filled with particles used in Monte Carlo simulations: 1 – incident radiation, 2 – diffusely reflected radiation, 3 – absorbed radiation, 4 – transmitted radiation, 5 – upper part of stratum corneum (1- μm -thick, with particles), 6 – lower part of stratum corneum (without particles). Thickness of the whole stratum corneum (5 and 6) is 20 μm .

We consider the integral characteristics of the registered radiation (over the whole surface or within the whole layer). The computational model of the stratum corneum consists of an infinitely wide plain layer, the upper part of which (1- μm -thick) contains TiO₂ (or Si) particles. Some authors try to take into account the real conditions representing the interfaces between the skin layers as quasi-random periodic structures (Meglinskii & Matcher 2002). The total thickness of both parts is 20 μm , which corresponds to the real dimension of this skin layer on the back

and arms (Bordenave *et al.* 2002); only the palms and soles have thicker stratum corneum (up to 150 μm) because of more intensive use of hands and feet (Caspers *et al.* 2003).

The Monte Carlo method was used to simulate the propagation of photons inside both parts of the horny layer. One million photons were injected into the skin. All results were normalized by this value. This amount ensured suitable calculation time of about 5 minutes for each set of parameters and a statistical error of less than 3%. Imaginary detectors were located on the outer sides of each part of the horny layer. The lowermost one separated the stratum corneum from the epidermis. Such tissue-detector localization *in vivo* can hardly be achieved noninvasively, making simulations very important. Some experiments were performed recently *in vivo* to reveal the protection effect of administered sunscreens, but they disturbed living tissue with detectors situated between epidermis and dermis (Lademann, Jacobi *et al.* 2004). The detectors collected photons moving from the horny layer into the air or epidermis. In this study, we considered only the “unshaded” effect of the horny layer with TiO_2 (or Si) nanoparticles added, not taking into account deeper localized skin layers as scattering and absorbing media. The epidermis affected only the mismatch of refractive indices between itself and the stratum corneum. It was not described by any optical parameters except the refractive index ($n_m = 1.5$) because all UV photons penetrating the epidermis were considered potentially dangerous for its viable cells. That is why the topically applied substances are used to decrease the amount of UV light transmitted through the horny layer. Further consideration of photon migration within the epidermis and lower layers was not involved in the study; but these layers could affect the total amount of radiation detected on the surface of the skin and inside it. In other words, UV photons penetrating the epidermis might also be scattered back into the stratum corneum without inflicting any damage. Once in the stratum corneum, they might (1) exit the skin into the air, thus becoming completely harmless, (2) be absorbed in the stratum corneum (adding to the temperature rise in there), or (3) get scattered back into the epidermis. Not only this could reduce the fluence level in the epidermis, but the ratios between the above mentioned three events could vary strongly with the particle diameter and light wavelength. In this study, the following components of the radiation were registered: the amount of photons totally reflected in the backward direction (detected on the surface of the skin), absorbed within each part of the stratum corneum with and without particles and transmitted both through the upper part and the whole horny layer.

Cells of the stratum corneum are known to be shaped as flat cylinders (Schaefer & Redelmeier 1996). Although they differ from other cells of internal skin layers such as epidermis and dermis, the Henyey-Greenstein (HG) phase function (Henyey & Greenstein 1941) seems to give a satisfactory characterization for the stratum corneum scattering behaviour in the UV region that was deduced from the comparison of experimental data and calculations results (Bruls & van der Leun 1984):

$$p_{HG}(\theta) = \frac{1}{4\pi} \cdot \frac{1-g^2}{(1+g^2-2g\cos\theta)^{3/2}}, \quad (4)$$

where g is the scattering anisotropy factor. The circumferential angle is defined as $\varphi = 2\pi\text{Random}$ (Cashwell & Everett 1959), where *Random* is a Delphi® software-generated random value, evenly distributed within the interval of [0, 1].

A superposition of the horny layer matrix (host medium) and particles embedded into it is considered in the model. These particles are of nano-size and assumed to be spherical. Light scattering from such particles is described by the Mie scattering phase function $p_{Mie}(\theta)$ (van de Hulst 1957) obtained by the software MieTab 7.23 mentioned above. The hybrid scattering phase function for the upper part of the horny layer (with the particles) used in these simulations is:

$$p(\theta) = R \cdot p_{Mie}(\theta) + (1-R) \cdot p_{HG}(\theta), \quad (5)$$

$$2\pi \int_0^\pi p(\theta) \sin(\theta) d\theta = 1, \quad (6)$$

where $R = \mu_s^{(1)} / (\mu_s^{(1)} + \mu_s^{(2)})$, $\mu_s^{(1)}$ is the scattering coefficient of the particles of the concentration C determined by the formula (2), $\mu_s^{(2)}$ is a scattering coefficient of the horny layer matrix. The expression (5) is a simplified form of the scattering phase function of a mixture of polydisperse particles, where each kind of particle has its own scattering phase function (Murant *et al.* 1998). The use of a linear combination of two phase functions is not unusual: previously, the HG function and an isotropic term were suggested to describe light scattering in human dermis (Jacques *et al.* 1987) and dental enamel and dentin (Fried *et al.* 1995), a modified HG function with a normalization factor was used for human brain and stomach (Thueller *et al.* 2003), while a double HG function – for white matter of a neonate brain (Kienle *et al.* 2001). The mean free path l_{ph} and a free path L of a photon are defined as

$$l_{ph} = (\mu_s^{(1)} + \mu_s^{(2)} + \mu_a^{(1)} + \mu_a^{(2)})^{-1}, \quad (7)$$

$$L = -l_{ph} \cdot \ln(1 - \text{Random}), \quad (8)$$

where $\mu_a^{(1)}$ is the absorption coefficient of the particles of the concentration C determined by the formula (3), $\mu_a^{(2)}$ is the absorption coefficient of the horny layer matrix. Optical properties of the matrix for the considered wavelengths are shown in Table 2 (van Gemert *et al.* 1989; Tuchin 2000). Interaction between a photon and an equivalent quasiparticle is simulated. A medium consisting of such quasiparticles combines optical properties of both the horny layer matrix and the nanoparticles. A quasiparticle can scatter or absorb an incident photon. The photon is scattered with the probability p_s determined as:

$$p_s = (\mu_s^{(1)} + \mu_s^{(2)}) / (\mu_s^{(1)} + \mu_a^{(1)} + \mu_s^{(2)} + \mu_a^{(2)}). \quad (9)$$

In any other case it is absorbed. A more detailed description of the algorithm can be found elsewhere (Popov *et al.* 2003). The volume concentration of the particles C used in the simulations was 1%.

Table 2. Optical properties of stratum corneum matrix for 310- and 400-nm UV radiation (van Gemert *et al.* 1989; Tuchin 2000).

λ , nm	μ_s , mm ⁻¹	μ_a , mm ⁻¹	g	n_m
310	240	60	0.9	1.53
400	200	23	0.9	1.53

8.3.2 Results of simulations

Figure 25 illustrates the dependences of absorption on particle diameters within the upper part of the stratum corneum where nanoparticles (TiO₂ or Si) are present. One can see that the curves on both parts of the figure have similar shapes as those in Fig. 23. Positions of the highest values of absorption also coincide with those from Fig. 23 except for the TiO₂ curve at 400-nm light: the most absorbing particles have diameters of 122 (not 126) nm. About 50% of the incident radiation is absorbed if optimal particles of both types are used. It is worth noting that titanium dioxide particles absorb 400-nm light very weakly (no more than 5% of the incident radiation).

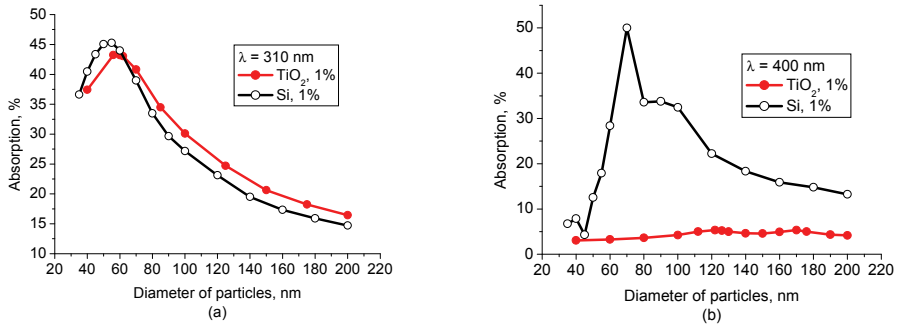


Fig. 25. Absorption of 310- (a) and 400-nm (b) light within the upper part of stratum corneum (with particles).

Reflectance from the whole stratum corneum (i.e. photons emerging from both part of the layer, with and without particles, registered on the surface of the layer) is depicted in Fig. 26.

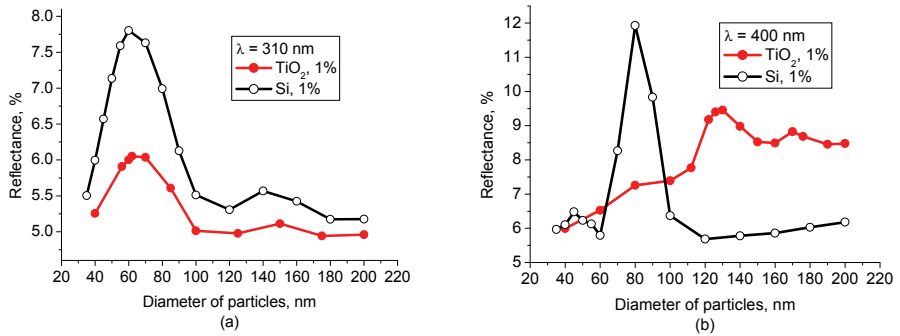


Fig. 26. Reflectance of 310- (a) and 400-nm (b) light from the whole stratum corneum in presence of TiO₂ or Si nanoparticles within its uppermost 1- μ m-thick part.

The reflection does not exceed 12% even for the most reflecting particles. The maxima are shifted by a couple of nm to the larger sizes in comparison to the curves in Fig. 23. This is explained in such a way that locations of the maxima of the extinction (Fig. 23) and scattering curves (not shown) do not coincide. If illuminated with the 310-nm light, reflectance is higher for silicon nanoparticles than for titanium dioxide ones for all considered sizes. If illuminated with the 400-nm light, smaller (up to 90 nm in diameter) Si particles reflect light better than TiO₂ ones; for larger (90–200 nm) sizes the situation is reverse.

If the particles are used as UV light protectors, their most important characteristic is how they attenuate radiation in all ways (both absorption and reflection). Transmittance of light of the two wavelengths is shown in Fig. 27. The curves look like inverted ones from Fig. 23, as they should be: the higher the extinction, the lower the transmittance. Three diameters of the most attenuating particles are coincident with those corresponding to the maxima in Fig. 23, namely 56 and 70 nm for Si (for 310- and 400-nm light, respectively) and 62 nm (for 310-nm light) for TiO₂ particles. A slight mismatch is observed for TiO₂ and 400-nm light: instead of 126 nm the optimal size is 122 nm. Nevertheless, it can be concluded that the extinction curves adequately describe the attenuation of light by particles. Simulation of UV light transmittance on emulsions with particles also showed that optimal Si particles are smaller than those of TiO₂ (VII).

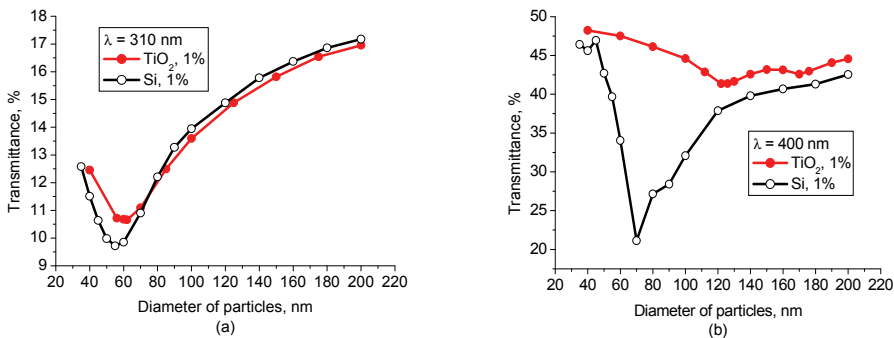


Fig. 27. Transmittance of 310- (a) and 400-nm (b) light through the whole stratum corneum in presence of TiO₂ or Si nanoparticles within its uppermost 1- μ m-thick part.

In Fig. 28 the comparison between the following three cases for 310- and 400-nm radiation is made: 1) stratum corneum without particles; 2) stratum corneum with optimal TiO₂ particles; 3) stratum corneum with optimal Si particles. The particles are located within the 1- μ m upper part of the stratum corneum, according to our model described above. Each column consists of the four components of the radiation (counting from the bottom): absorbed within the upper part (with particles), absorbed within the lower part (without particles), reflected from the whole stratum corneum and transmitted through the whole stratum corneum (entering epidermis located beneath the stratum corneum).

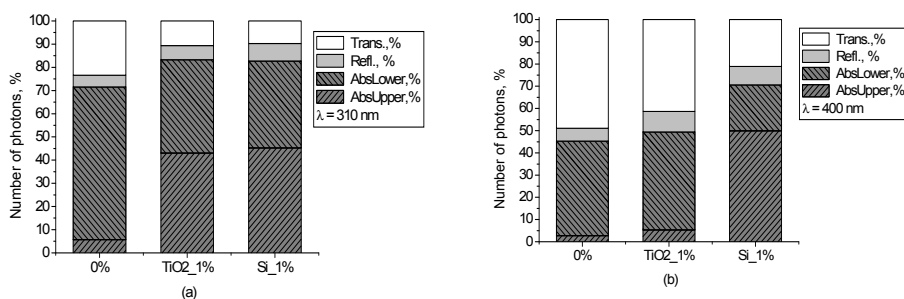


Fig. 28. Effect of the optimal TiO₂ and Si nanoparticles homogeneously distributed within the uppermost 1- μ m-thick part of the stratum corneum for 310- (a) and 400-nm (b) light.

Consider first the case of 310-nm radiation (Fig. 28 (a)). If particles of any of two types are added, absorption increases dramatically in the upper part (from 5 to 40%), almost to the same level. The increase in absorption in this part causes its decrease in the lower part (from 65% to 40% of the incident radiation). Nevertheless, the total absorption increases (from 70% to 85%) in the presence of the particles. Reflectance also increases. Because of these two factors, transmittance decreases from more than 20 to around 10%.

The difference between the effects of the two types of optimal particles is more pronounced if the radiation with the wavelength of 400 nm is considered (Fig. 28 (b)). TiO₂ particles are weak absorbers and the absorption in the upper part does not differ much from that of the stratum corneum without particles (still some synergy exists between the particles and the stratum corneum increasing absorbed radiation (Lademann, Schanzer *et al.* 2005)); their main contribution to light attenuation is caused by increased reflection (from 5% to 10%). In contrast to this, Si particles are such effective absorbers at this wavelength that the absorption in the upper part exceeds the absorption in the whole stratum corneum without particles or with TiO₂ particles. The reflection is of the same level as for titanium dioxide particles. The discussed reasons result in the transmittance values: about 45% and 20% in the presence of TiO₂ and Si particles respectively.

In the experiment carried out to compare its results with the simulations, the transmittance of UV light through a layer of o/w emulsion (L'Oréal, France) with nanoparticles UV-TITAN M 160 (Kemira, Finland) was measured with the spectrophotometer Lambda 20 (Perkin Elmer, Germany). In the corresponding simulations, 100-nm TiO₂ nanoparticles with a volume fraction of 0.2% embedded

into a 20- μm layer of the transparent medium with $n_m = 1.4$ were considered. Such a low concentration was chosen to be within the frames of independent scattering for all wavelength of the spectrum (288–800 nm). In all simulations one million photons were launched into the medium. This amount ensured sufficient statistical precision of the calculation with an error not exceeding 3%. Those photons that went out of the medium were collected at the following angles: azimuthal 0–360 degrees; polar: 0–90 degrees for the photons detected in the forward hemisphere, 90–180 degrees for those detected in the backward hemisphere, the polar angle is calculated relative to the direction of photon-incidence to the skin. The medium was assumed to be isotropic in the lateral directions.

Comparison between the experimental and simulation results for TiO_2 particles of average size of 100 nm is shown in Fig. 29 (a).

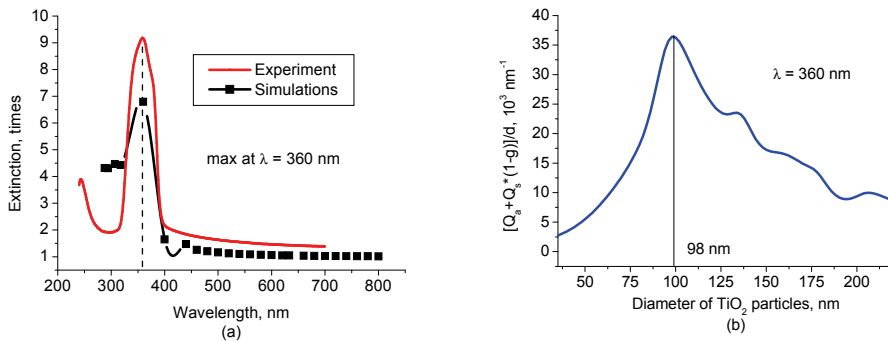


Fig. 29. Experimental and simulation attenuation curves (a) and dependence of quantity $[Q_a + Q_s(1 - g)]/d$ on a particle diameter for 360-nm light calculated using the Mie theory (b).

The curves represent the extinction (reciprocal to transmittance) in dependence on the wavelength. The discrepancy between the experimental and simulation curves is caused by the assumption of medium transparency and lower particle concentration (0.2%) used for simulations. The assumption of medium transparency was used because the absorption coefficient of the emulsion was not known. Some important features can be revealed from the experimental curve. As seen, the maximal extinction is achieved at the wavelength of 360 nm. By using the Mie theory, and taking into account the optical parameters of TiO_2 particles at 360-nm light ($n_p = 3.54$, $k_p = 0.16$ (Palik 1985)), a quantity representing a combination of relative scattering and absorption efficiency factor, g -factor and

particle diameter was calculated for the diameters of 35–200 nm and depicted in Fig. 29 (b). The position of the maximum of the drawn curve indicates the size of the most attenuating particles (VI). In our case it is 98 nm. Using the optical parameters of the TiO₂ particles for UV and visible spectral ranges (Table 3), the relative scattering and absorption efficiency factors as well as *g*-factor, a simulation curve was calculated (Fig. 29 (a)). The maxima of the both curves in Fig. 29 (a) clearly coincide. This proves that the size of nanoparticles embedded in the emulsion in the experiment was about 100 nm.

Table 3. Optical parameters of TiO₂ particles in UV and visible spectrum ranges (Palik 1985).

Wavelength, nm	Refractive index		Wavelength, nm	Refractive index	
	<i>Re</i> (<i>n_p</i>)	<i>Im</i> (<i>n_p</i>)		<i>Re</i> (<i>n_p</i>)	<i>Im</i> (<i>n_p</i>)
288	3.07	2.40	580	2.72	0
294	3.42	2.47	600	2.70	0
307	3.56	1.72	620	2.69	0
318	4.46	1.92	633	2.68	0
360	3.54	0.16	660	2.66	0
400	3.13	0.008	680	2.65	0
440	2.96	0.053	700	2.64	0
460	2.90	0	720	2.63	0
480	2.86	0	740	2.63	0
500	2.82	0	760	2.62	0
520	2.79	0	780	2.61	0
540	2.76	0	800	2.61	0
560	2.74	0			

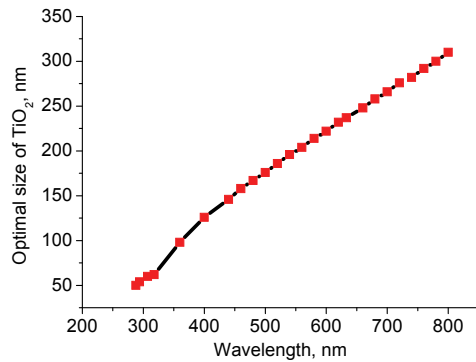


Fig. 30. Optimal sizes of TiO₂ imbedded into the stratum corneum.

Figure 30 represents the dependence of optimal diameters (from the viewpoint of light attenuation) of TiO₂ particles, embedded in the stratum corneum, on the wavelengths. The dependence is close to being linear: the larger the light wavelength – the larger the TiO₂ particles should be to attenuate light in the optimal way. This prediction is also supported by the simulations of OCT signals from the stratum corneum partially filled with TiO₂ particles (Popov, Kirillin *et al.* 2005): for 633-nm light, the weakest signal from the rear border of the layer was observed for the sizes of 200-nm (the largest size of all considered).

9 Summary

In tape stripping experiments with the porcine ear skin, it is shown experimentally that there is a linear dependence between the absorbance (equals to logarithm of inverse transmittance) and thickness of the corneocytes on tape strips for all wavelengths of the investigated region (300–1050 nm). Thus, it is possible to replace the time-consuming weighing procedure with the spectroscopic measurements. Dependence of the cumulative absorbance of the removed stratum corneum on tape strip number can be satisfactorily fitted by an exponential function. This relationship allows an evaluation of the relative share of the removed stratum corneum, without complete removal of this layer. All the obtained results correlate well with those obtained on humans. Applied laser scanning fluorescence microscopy to corneocytes imaging, qualitative similarities between forms and sizes of porcine and human cells are found.

As proved experimentally by means of EPR spectroscopy, small (25 nm in diameter) coated nanoparticles of titanium dioxide (anatase form) are more photoactive than large (400 nm in diameter) particles. This effect is clearly seen if the particles embedded into placebo are applied on glass. The Mie theory explains the difference in light absorption by particles of the mentioned sizes and, as a consequence, the difference in amount of generated free radicals. However, if the particles are applied onto the porcine skin *in vitro*, no distinct difference is observed. This is caused by high skin contribution to the generation of radicals. In comparison to the skin's ability to produce radicals, the nanoparticles do not play a significant role in the concentrations used (2 mg cm^{-2}).

The modification of skin optical properties by means of application of nanoparticles of two types (TiO_2 (rutile form) and Si) is investigated by implementing the Mie theory and Monte Carlo simulations. For the two wavelengths of light considered, the sizes of the most attenuating particles are the following: 56 and 70 nm for Si and 62 and 122 nm for TiO_2 particles (for 310- and 400-nm light, respectively). The mechanisms behind these effects are absorption of the UV radiation of the shorter wavelength radiation for the both types of the particles; scattering for TiO_2 and absorption and to a lesser extent scattering for Si nanoparticles of the longer wavelength light. Although the possible existence of SiO_2 shells on the particles was not taken into account in the calculations, the effect of extinction is more pronounced in this case because the real part of the refractive index of SiO_2 is 1.47–1.49 for the radiation of 290–400 nm and hence is lower than that of skin (1.53).

References

- Ahonen PP, Joutensaari J, Richard O, Tapper U, Brown D, Jokiniemi J & Kauppinen E (2001) Mobility size development and the crystallization path during aerosol decomposition synthesis of TiO₂ particles. *J Aerosol Sci* 32: 615–630.
- Alberti I, Kalia YN, Naik A, Bonny J-D & Guy RH (2001) In vivo assessment of enhanced topical delivery of terbinafine to human stratum corneum. *J Control Release* 71: 319–327.
- Ananthaswamy HN & Pierceall WE (1990) Molecular mechanisms of ultraviolet radiation carcinogenesis. *Photochem Photobiol* 52: 1119–1136.
- Anderson RL & Cassidy JM (1973) Variations in physical dimensions and chemical composition of human stratum corneum. *J Invest Dermatol* 61: 30–32.
- Bakarjieva S, Šubr J, Štengl V, Dianez MJ & Sayagues MJ (2005) Photoactivity of anatase-rutile TiO₂ nanocrystalline mixtures obtained by heat treatment of homogeneously precipitated anatase. *Appl Catal B: Environmental* 58: 193–202.
- Bartek MJ, LaBudde JA & Maibach HI (1972) Skin permeability in vivo: comparison in rat, rabbit, pig and man. *J Invest Dermatol* 58: 114–123.
- Bommann D, Potts RO & Guy RH (1990) Examination of stratum corneum barrier function in vivo by infrared spectroscopy. *J Invest Dermatol* 95: 403–408.
- Bordenave E, Abraham E, Jonusauskas G, Tsurumach N, Oberlé J, Rullière C, Minot PE, Lassègues M & Surlève Bazeille JE (2002) Wide-field optical coherence tomography: imaging of biological tissues. *Appl Opt* 41: 2059–2064.
- Bouwstra JA, de Graaf A, Gooris GS, Nijse J, Wichers JW & van Aelst AC (2003) Water distribution and related morphology in human stratum corneum at different hydration levels. *J Invest Dermatol* 120: 750–758.
- Bouwstra JA, Gooris GS, Weerheim A, Kempenaar J & Ponc M (1995) Characterization of stratum corneum structure in reconstructed epidermis by X-ray diffraction. *J Lipid Res* 36: 496–504.
- Bruls WAG & van der Leun JC (1984) Forward scattering properties of human epidermal layers. *Photochem Photobiol* 40: 231–242.
- Bruls WAG, Slaper H, van der Leun JC & Berrens L (1984) Transmission of human epidermis and stratum corneum as a function of thickness in the ultraviolet and visible wavelengths. *Photochem Photobiol* 40: 485–494.
- Cao L, Huang A, Spiess F-J & Suib SL (1999) Gas-phase oxidation of 1-butene using nanoscale TiO₂ photocatalysts. *J Catal* 188: 48–57.
- Cashwell ED & Everett CJ (1959) *A Practical Manual on the Monte Carlo Method for Random Walk Problems*. New York: Pergamon Press.
- Caspers PJ, Lucassen GW & Puppels GJ (2003) Combined in vivo confocal Raman spectroscopy and confocal microscopy of human skin. *Biophys J* 85: 572–580.
- Cheong W-F, Prah SA & Welch AJ (1990) A review of the optical properties of biological tissues. *IEEE J Quantum Electr* 26: 2166–2185.
- Christophers E (1971) Cellular architecture of the stratum corneum. *J Invest Dermatol* 56: 165–169.

- COLIPA, European Cosmetic, Toiletry and Perfumery Association (1994) COLIPA sun protection factor test method 94/289.
- Collins B, Poehler TO & Bryden WA (1995) EPR persistence measurements of UV-induced melanin free radicals in whole skin. *Photochem Photobiol* 62: 557–560.
- Darr D & Fridovich I (1994) Free radicals in cutaneous biology. *J Invest Dermatol* 102: 671–675.
- Darvin ME, Gersonde I, Albrecht H, Sterry W & Lademann J (2006) In vivo Raman spectroscopic analysis of the influence of UV radiation on carotenoid antioxidant substance degradation of the human skin. *Laser Phys* 16: 833–837.
- Darvin ME, Gersonde I, Meinke M, Sterry W & Lademann J (2005) Noninvasive in vivo determination of the carotenoids beta-carotene and lycopene concentrations in the human skin using the Raman spectroscopic method. *J Phys D: Appl Phys* 38: 2696–2700.
- Darwin M, Schanzer S, Teichmann A, Blume-Peytavi U, Sterry W & Lademann J (2006) Functional Food und Bioverfügbarkeit im Zielorgan Haut. *Hautarzt* 57: 286–290.
- Davies H, Bignell GR, Cox C, Stephens P, Edkins S, Clegg S, Teague J, Woffendin H, Garnett MJ, Bottomley W, Davis N, Dicks E, Ewing R, Floyd Y, Gray K, Hall S, Hawes R, Hughes J, Kosmidou V, Menzies A, Mould C, Parker A, Stevens C, Watt S, Hooper S, Wilson R, Jayatilake H, Gusterson BA, Cooper C, Shipley J, Hargrave D, Pritchard-Jones K, Maitland N, Chenevix-Trench G, Riggins GJ, Bigner DD, Palmieri G, Cossu A, Flanagan A, Nicholson A, Ho JWC, Leung SY, Yuen ST, Weber BL, Seigler HF, Darrow TL, Paterson H, Marais R, Marshall CJ, Wooster R, Stratton MR & Futreal PA (2002) Mutations of the BRAF gene in human cancer. *Nature* 417: 949–954.
- Diebold U (2003) The surface science of titanium dioxide. *Surf Sci Rep* 48: 53–229.
- Diffey B (2004) Climate change, ozone depletion and the impact on ultraviolet exposure of human. *Phys Med Biol* 49: R1–R11.
- Diffey BL (1991) Solar ultraviolet radiation effects on biological systems. *Phys Med Biol* 36: 299–328.
- Dröge W (2002) Free radicals in the physiological control of cell function. *Physiol Rev* 82: 47–95.
- Dunford R, Salinaro A, Cai L, Serpone N, Horikoshi S, Hidaka H & Knowland J (1997) Chemical oxidation and DNA damage catalysed by inorganic sunscreen ingredients. *FEBS Lett* 418: 87–90.
- Edlich RF, Winter KL, Lim HW, Cox MJ, Becker DG, Horovitz JH, Nichter LS, Britt LD & Long WB (2004) Photoprotection by sunscreens with topical antioxidants and systematic antioxidants to reduce sun exposure. *J Long-Term Effects Med Implants* 14: 317–340.
- Ferrero L, Pissavini M & Zastrow L (1999) Spectroscopy of sunscreen products. *Proc European UV Sunfilters Conference*. Paris, France: 52–64.
- Fried D, Glena RE, Featherstone JDB & Seka W (1995) Nature of light scattering in dental enamel and dentin at visible and near-infrared wavelengths. *Appl Opt* 34: 1278–1285.
- Fritsch P (1998) *Dermatologie und Venerologie*. Berlin-Heidelberg: Springer-Verlag.

- Fuchs J, Herrling T & Groth N (2001) Detection of free radicals in skin: a review of the literature and new developments. In: Thiele J & Elsner P (eds) *Oxidants and antioxidants in cutaneous biology*. Basel, Karger: 1–17.
- Garidel P (2002) Mid-FTIR-microspectroscopy of stratum corneum single cells and stratum corneum tissue. *Phys Chem Chem Phys* 4: 5671–5677.
- Gueymard CA, Myers D & Emery K (2002) Proposed reference irradiance spectra for solar energy systems testing. *Solar Energy* 73: 443–467.
- Haag S (2007) Nachweis von freien Radikalen in biologischen Proben mittels ESR-Spektroskopie. MSc. thesis. Technical University Berlin.
- Henyeu LG & Greenstein JL (1941) Diffuse radiation in the galaxy. *Astrophys J* 93: 70–83.
- Herrling T, Fuchs J & Groth N (2002) Kinetic measurements using EPR imaging with a modulated field gradient. *J Magn Reson* 154: 6–14.
- Herrling T, Fuchs J, Rehberg J & Groth N (2003) UV-induced free radical in the skin detected by ESR spectroscopy and imaging using nitroxides. *Free Radic Biol Med* 35: 59–67.
- Herrling T, Jung K & Fuchs J (2005) Measurements of UV-generated free radicals/reactive oxygen species (ROS) in skin. *Spectrochim Acta A* 63: 840–845.
- Herrling T, Zastrow L, Fuchs J & Groth N (2002) Electron spin resonance detection of UVA-induced free radicals. *Skin Pharmacol Appl Skin Physiol* 15: 381–383.
- Hidaka H, Horikoshi S, Serpone N & Knowland J (1997) In vitro photochemical damage to DNA, RNA and their bases by an inorganic sunscreen agent on exposure to UVA and UVB radiation. *J Photochem Photobiol A: Chem* 111: 205–213.
- Holbrook KA & Odland GF (1974) Regional differences in the thickness (cell layers) of the human stratum corneum: an ultrastructural analysis. *J Invest Dermatol* 62: 415–422.
<http://amiller.nmsu.edu/mietab.html>
- Innes B, Tsuzuki T, Dawkins H, Dunlop J, Trotter G, Nearn MR & McCormick PG (2002) Nanotechnology and the cosmetic chemist. *Cosmetics, Aerosols and Toiletries in Australia* 15: 10–12, 21–24.
- Jackson KDO (1998) A guide to identifying common inorganic fillers and activators using vibrational spectroscopy. *The Internet Journal of Vibrational Spectroscopy* 3
<http://www.ijvs.com/volume2/edition3/section3.html#jackson>
- Jacobi U, Chen M, Frankowski G, Sinkgraven R, Hund M, Rzany B, Sterry W & Lademann J (2004) In vivo determination of skin surface topography using an optical 3D device. *Skin Res Technol* 10: 207–214.
- Jacobi U, Kaiser M, Richter H, Audring H, Sterry W & Lademann J (2005) The number of stratum corneum cell layers correlates with the pseudo-absorption of the corneocytes. *Skin Pharmacol Physiol* 18: 175–179.
- Jacobi U, Kaiser M, Toll R, Mangelsdorf S, Audring H, Otberg N, Sterry W & Lademann J (2007) Porcine ear skin: an in vitro model for human skin. *Skin Res Tech* 13: 19–24.
- Jacobi U, Meykadeh N, Sterry W & Lademann J (2003) Effect of the vehicle on the amount of stratum corneum removed by tape stripping. *J Dt Dermatol Gesell* 1: 884–889.
- Jacobi U, Toll R, Audring H, Sterry W & Lademann J (2005) The porcine snout – an in vitro model for human lips. *Experiment Dermatol* 14: 96–102.

- Jacobi U, Toll R, Sterry W & Lademann J (2005) Do follicles play a role as penetration pathways in in vitro studies on porcine skin? – An optical study. *Laser Phys* 15: 1594–1598.
- Jacobi U, Waibler E, Bartoll J, Schulze P, Sterry W & Lademann J (2004) In vivo determination of doxorubicin and its metabolites within the skin using laser scanning microscopy. *Laser Phys Lett* 1: 100–103.
- Jacobi U, Waibler E, Sterry W & Lademann J (2005) In vivo determination of the long-term reservoir of the horny layer using laser scanning microscopy. *Laser Phys* 15: 565–569.
- Jacobi U, Weigmann H-J, Baumann M, Reiche A-I, Sterry W & Lademann J (2004) Lateral spreading of topically applied UV filter substances investigated by tape stripping. *Skin Pharmacol Physiol* 17: 17–22.
- Jacobi U, Weigmann H-J, Ulrich J, Sterry W & Lademann J (2005) Estimation of the relative stratum corneum amount removed by tape stripping. *Skin Res Tech* 11: 91–96.
- Jacques SL, Alter CA & Prael SA (1987) Angular dependence of HeNe laser light scattering by human dermis. *Las Life Sci* 1: 309–333.
- Jellison Jr GE, Boatner LA & Budai JD (2003) Spectroscopic ellipsometry of thin film and bulk anatase (TiO₂). *J Appl Phys* 93: 9537–9541.
- Kakinoki K, Yamane K, Teraoka R, Otsuka M & Matsuda Y (2004) Effect of relative humidity on the photocatalytic activity of titanium dioxide and photostability of famotidine. *J Pharm Sci* 93: 582–589.
- Kalia YN, Alberti I, Sekkat N, Curdy C, Naik A & Guy R (2000) Normalization of stratum corneum barrier function and transdermal water loss in vivo. *Pharm Res* 17: 1148–1150.
- Kalia YN, Pirot F & Guy RH (1996) Homogeneous transport in a heterogeneous membrane: water diffusion across human stratum corneum in vivo. *Biophys J* 71: 2692–2700.
- Kawasaki Y, Quan D, Sakamoto K, Cooke R & Maibach HI (1999) Influence of surfactant mixtures on intercellular lipid fluidity and skin barrier function. *Skin Res Technol* 5: 96–101.
- Kienle A, Forster FK & Hibst R (2001) Influence of the phase function on determination of the optical properties of biological tissue by spatially resolved reflectance. *Opt Lett* 26: 1571–1573.
- Lademann J, Ingevicus A, Zurbau O, Liess HD, Schanzer S, Weigmann H-J, Antoniou C, von Pelchrzim R & Sterry W (2006). Penetration studies of topically applied substances: optical determination of the amount of stratum corneum removed by tape stripping. *J Biomed Opt* 11: 054026-1-6.
- Lademann J, Jacobi U, Richter H, Otberg N, Weigmann H-J, Meffert H, Schaefer H, Blueme-Peytavi U & Sterry W (2004) In vivo determination of UV-photons entering into human skin. *Laser Phys* 14: 234–237.
- Lademann J, Knüttel A, Richter H, Otberg N, v Pelchrzim R, Audring H, Meffert H, Sterry W & Hoffmann K (2005) Application of optical coherent tomography for skin diagnostics. *Laser Phys* 15: 288–294.
- Lademann J, Richter H, Otberg N, Lawrenz F, Blume-Peytavi U & Sterry W (2003) Application of a dermatological laser scanning confocal microscope for investigation in skin physiology. *J Laser Phys* 13: 756–760.

- Lademann J, Rudolph A, Jacobi U, Weigmann H-J, Schafer H, Sterry W & Meinke M (2004) Influence of nonhomogeneous distribution of topically applied UV filters on sun protection factors. *J Biomed Opt* 9: 1358–1362.
- Lademann J, Schanzer S, Jacobi U, Schaefer H, Pflücker F, Driller H, Beck J, Meinke M, Roggan A & Sterry W (2005) Synergy effects between organic and inorganic UV filters in sunscreens. *J Biomed Opt* 10: 014008-1-7.
- Lademann J, Weigmann H-J, Rickmeyer C, Barthelmes H, Schaefer H, Mueller G & Sterry W (1999) Penetration of titanium dioxide microparticles in a sunscreen formulation into the horny layer and the follicular orifice. *Skin Pharmacol Appl Skin Physiol* 12: 247–256.
- Lademann J, Weigmann H-J, Schaefer H, Mueller G & Sterry W (2000) Investigation of the stability of coated titanium microparticles used in sunscreens. *Skin Pharmacol Appl Skin Physiol* 13: 258–264.
- Lademann J, Weigmann H-J, Schanzer S, Richter H, Audring H, Antoniou C, Tsirikas G, Gers-Barlag H & Sterry W (2005) Optical investigations to avoid the disturbing influences of furrows and wrinkles quantifying penetration of drugs and cosmetics into the skin by tape stripping. *J Biomed Opt* 10: 054015-1-8.
- Lindemann U, Weigmann H-J, Schaefer H, Sterry W & Lademann J (2003) Evaluation of the pseudo-absorption method to quantify human stratum corneum removed by tape stripping using protein absorption. *Skin Pharmacol Appl Skin Physiol* 16: 228–236.
- Lindemann U, Wilken K, Weigmann H-J, Schaefer H, Sterry W & Lademann J (2003) Quantification of the horny layer using tape stripping and microscopic techniques. *J Biomed Opt* 8: 601–607.
- McKinlay AF & Diffey BL (1987a) A reference action spectrum for ultraviolet induced erythema in human skin. *CIE J* 6: 17–22.
- McKinlay AF & Diffey BL (1987b) A reference action spectrum for ultraviolet induced erythema in human skin. In: Passchier BF & Bosnjakovic BFM (eds) *Human Exposure to Ultraviolet Radiation: Risks and Regulations*. Amsterdam, Elsevier: 83–87.
- McNeil LE & French RH (2000) Multiple scattering from rutile TiO₂ particles. *Acta Mater* 48: 4571–4576.
- Meglinskii IV & Matcher SJ (2002) Quantitative assessment of skin layers absorption and skin reflectance spectra simulation in visible and near-infrared spectral region. *Physiol Meas* 23: 741–753.
- Meinke M, Haag S, Groth N, Klein F, Lauster R, Sterry W & Lademann J (2008) Method for detection of free radicals in skin by EPR spectroscopy after UV irradiation. *SÖFW-Journal* 3: 2–10.
- Meyer LE, Otberg N, Richter R, Sterry W & Lademann J (2006) New prospects in dermatology: fiber-based confocal scanning laser microscopy. *Laser Phys* 16: 758–764.
- Meyer LE, Otberg N, Tietz H-J, Sterry W & Lademann J (2004) In vivo imaging of Malassezia yeasts on human skin using confocal laser scanning microscopy. *Laser Phys Lett* 2: 148–152.
- Mosteller RD (1987) Simplified calculation of body surface area. *N Engl Med* 317: 1098.

- Murant JR, Freyer JP, Hielscher AH, Eick AA, Shen D & Johnson TM (1998) Mechanisms of light scattering from biological cells relevant to noninvasive optical-tissue diagnostics. *Appl Opt* 37: 3586–3593.
- Nishi J, Ogura R, Sugiyama M, Hidaka T & Kohno M (1991) Involvement of active oxygen in lipid peroxide radical reaction of epidermal homogenate following ultraviolet light exposure. *J Invest Dermatol* 97: 115–119.
- Ogura R, Sugiyama M, Nishi J & Haramaki N (1991) Mechanism of lipid formation following exposure of epidermal homogenate to ultraviolet light. *J Invest Dermatol* 97: 1044–1047.
- Otberg N, Richter H, Schaefer H, Blume-Peytavi U, Sterry W & Lademann J (2004) Variations of hair follicle size and distribution in different body sites. *J Invest Dermatol* 122: 14–19.
- Otberg N, Richter H, Schaefer H, Blume-Peytavi U, Sterry W & Lademann J (2003) Visualization of topically applied fluorescent dyes in hair follicles by laser scanning microscopy. *Laser Phys* 13: 761–764.
- Otberg N, Richter H, Knuttel, Schaefer H, Sterry W & Lademann J (2004) Laser spectroscopic methods for the characterization of open and closed follicles. *Laser Phys Lett* 1: 46–49.
- Palik ED (1985) *Handbook of Optical Constants of Solids*. Orlando: Academic Press.
- Palmer BR, Stamatakis P, Bohren CF & Salzman GC (1989) A multiple scattering model for opacifying particles in polymer films. *J Coat Technol* 61: 41–47.
- Pilgram GSK, Engelsma-van Pelt AM, Oostergetel GT, Koerten HK & Bouwstra JA (1998) Study on the lipid organization of stratum corneum lipid models by (cryo-) electron diffraction. *J Lipid Res* 39: 1669–1676.
- Popov A, Lademann J & Myllylä R (2008) Titanium dioxide nanoparticles in sunscreens: generation of free radicals under UV irradiation. *Proc International Conference “Optics Days”*. Kuopio, Finland: 38.
- Popov AP & Priezzhev AV (2003) Laser pulse propagation in turbid media: Monte Carlo simulation and comparison with experiment. *Proc SPIE* 5068: 299–308.
- Popov AP, Kirillin MY, Priezzhev AV, Lademann J, Hast J & Myllylä R (2005) Optical sensing of titanium dioxide nanoparticles within horny layer of human skin and their protecting effect against solar UV radiation. *Proc. SPIE* 5702: 113–122.
- Popov AP, Priezzhev AV, Lademann J & Myllylä R (2005) Efficiency of TiO₂ nanoparticles of different sizes as UVB light skin-protective fraction in sunscreens. *Proc. SPIE* 5771: 336–343.
- Popov AP, Priezzhev AV, Lademann J & Myllylä R (2006a) Advantages of NIR radiation use for optical determination of skin horny layer thickness with embedded TiO₂ nanoparticles during tape stripping procedure. *Laser Phys* 16: 751–757.
- Popov AP, Priezzhev AV, Lademann J & Myllylä R (2006b) The effect of nanometer particles of titanium oxide on the protective properties of skin in the UV region. *J Opt Technol* 73: 208–211.

- Popov AP, Priezzhev AV, Lademann J & Myllylä R (2007) Influence of multiple light scattering on TiO₂ nanoparticles imbedded into stratum corneum, on light transmittance in UV and visible wavelength regions. *Proc. SPIE* 6535: 65351E–1–6.
- Rieger T, Teichmann A, Richter H, Sterry W & Lademann J (2007) Application of in-vivo laser scanning microscopy for evaluation of barrier creams. *Laser Phys Lett* 4: 72–76.
- Riemann I, Dimitrow E, Fischer P, Reif A, Kaatz M, Elsner P & König K (2004) High resolution multiphoton tomography of human skin in vivo and in vitro. *Proc SPIE* 5463: 21–28.
- Rybaltofsky AI, Bagratashvili VN, Belogorokhov AI, Koltashev VV, Plotnichenko VG, Popov AP, Priezzhev AV, Ishchenko AA, Sviridova AA, Zatseva KV & Tutorsky IA (2006) Spectral features of water-emulsion composite media containing silicon nanoparticles. *Optics and Spectroscopy* 101: 590–596.
- Schaefer H & Redelmeier T (1996) *Skin Barrier: Principles of Percutaneous Absorption*. Basel: Karger.
- Schwindt DA, Wilhelm KP & Maibach HI (1998) Water diffusion characteristics of human stratum corneum at different anatomical sites in vivo. *J Invest Dermatol* 111: 385–389.
- Setlow RB (1974) The wavelengths in sunlight effective in producing skin cancer: a theoretical analysis. *Proc Nat Acad Sci USA* 71: 3363–3366.
- Setlow RB, Grist E, Thompson K & Woodhead AD (1993) Wavelengths effective in induction of malignant melanoma. *Proc Nat Acad Sci* 90: 6666–6670.
- Shao Y & Slossmann D (1999) Effect of particle size on performance of physical sunscreen formulas. *Proc Personal Care Ingredients Asia Conference*. Shanghai, P.R. China: 1–9.
- Simon GA & Maibach HI (2000) The pig as an experimental animal model of percutaneous permeation in man: qualitative and quantitative observations – an overview. *Skin Pharmacol Appl Skin Physiol* 13: 229–234.
- Teichmann A, Jacobi U, Ossadnik M, Richter H, Koch S, Sterry W & Lademann J (2005) Differential stripping: determination of the amount of topically applied substances penetrated into the hair follicles. *J Invest Dermatol* 125: 264–269.
- Teichmann A, Sadeyh Pour Soleh H, Schanzer S, Richter H, Schwarz A & Lademann J (2006) Evaluation of the efficacy of skin care products by laser scanning microscopy. *Laser Phys Lett* 3: 507–509.
- Thueller P, Charvet I, Bevilacqua F, Ghislain MSt, Ory G, Marquet P, Meda P, Vermeulen B & Depeursinge C (2003). In vivo endoscopic tissue diagnostics based on spectroscopic absorption, scattering, and phase function properties. *J Biomed Opt* 8: 495–503.
- Tuchin VV (2000) *Tissue Optics*. Bellingham: SPIE Press.
- Tuchin VV (2002) *Handbook of Optical Biomedical Diagnostics*. Bellingham: SPIE Press.
- Van de Hulst HC (1957) *Light scattering by small particles*. New York: Wiley.
- Van Gemert MJC, Jacques SL, Sterenborg HJCM & Star VM (1989) *Skin Optics*. IEEE Trans Biomed Eng 36: 1146–1154.
- Vorontsov AV, Altyinnikov AA, Savinov EN & Kurkin EN (2001) Correlation of TiO₂ photocatalytic activity and diffuse reflectance spectra. *J Photochem Photobiol A: Chem* 144: 193–196.

- Warner WG, Yin J-J & Wei RR (1997) Oxidative damage to nucleic acids photosensitized by titanium dioxide. *Free Radic Biol Med* 23: 851–858.
- Watson SS, Beydoun D, Scott JA & Amal R (2003) The effect of preparation method on the photoactivity of crystalline titanium dioxide particles. *Chem Eng J* 95: 213–220.
- Weigmann H-J, Jacobi U, Antoniou C, Tsikrikas G, Wendel V, Rapp C, Gers-Barlag H, Sterry W & Lademann J (2005) Determination of penetration profiles of topically applied substances by means of tape stripping and optical spectroscopy: UV filter substance in sunscreen. *J Biomed Opt* 10: 014009-1-7.
- Weigmann H-J, Lademann J, Meffert H, Schaefer H & Sterry W (1999) Determination of the horny layer profile by tape stripping in combination with optical spectroscopy in the visible range as a prerequisite to quantify percutaneous absorption. *Skin Pharmacol Appl Skin Physiol* 12: 34–45.
- Weigmann H-J, Lademann J, Schanzer S, Lindemann U, von Pelchrzim R, Schaefer H, Sterry W & Shah V (2001) Correlation of the local distribution of topically applied substances inside the stratum corneum determined by tape-stripping to differences in bioavailability. *Skin Pharmacol App Skin Physiol* 14: 98–102.
- Weigmann H-J, Lindemann U, Antoniou C, Tsikrikas GN, Stratigos AI, Katsambas A, Sterry W & Lademann J (2003) UV/VIS absorbance allows rapid, accurate, and reproducible mass determination of corneocytes removed by tape stripping. *Skin Pharmacol App Skin Physiol* 16: 217–227.
- Weigmann H-J, Ulrich J, Schanzer S, Jacobi U, Schaefer H, Sterry W & Lademann J (2005) Comparison of transepidermal water loss and spectroscopic absorbance to quantify changes of the stratum corneum after tape stripping. *Skin Pharmacol Physiol* 18: 180–185.
- www.millenniumchem.com
- www.mydr.com.au
- Young AR (1997) Chromophores in human skin. *Phys Med Biol* 42: 789–802.
- Zhang Z, Wang C-C, Zakaria R & Ying JY (1998) Role of particle size in nanocrystalline TiO₂-based photocatalysts. *J Phys Chem B* 102: 10871–10878.

Original papers

- I Popov AP, Lademann J, Priezzhev AV & Myllylä R (2007) Reconstruction of stratum corneum profile of porcine ear skin after tape stripping using UV/VIS spectroscopy. *Proc SPIE* 6628: 66281S–1–6. DOI: 10.1117/12.729525.
- II Popov AP, Priezzhev AV, Lademann J & Myllylä R (2004) Manipulation of optical properties of human skin by light scattering nanoparticles of titanium dioxide. *Proc SPIE* 5578: 269–277. DOI: 10.1117/12.567423.
- III Popov AP, Priezzhev AV & Lademann J (2005) Control of optical properties of human skin by embedding light scattering nanoparticles. *Proc SPIE* 5850: 286–293. DOI: 10.1117/12.633742.
- IV Popov AP, Priezzhev AV, Lademann J & Myllylä R (2005) TiO₂ nanoparticles as an effective UV-B radiation skin-protective compound in sunscreens. *J Phys D: Appl Phys* 38: 2564–2570. DOI: 10.1088/0022-3727/38/15/006.
- V Popov AP, Lademann J, Priezzhev AV & Myllylä R (2005) Effect of size of TiO₂ nanoparticles embedded into stratum corneum on ultraviolet-A and ultraviolet-B sun-blocking properties of the skin. *J Biomed Opt* 10: 064037–1–9. DOI: 10.1117/1.2138017.
- VI Popov AP, Priezzhev AV, Lademann J & Myllylä R (2007) Effect of multiple scattering of light by titanium dioxide nanoparticles implanted into a superficial skin layer on radiation transmission in different wavelength ranges. *Quantum Electron* 37: 17–21. DOI: 10.1070/QE2007v037n01ABEH013461.
- VII Popov AP, Priezzhev AV, Lademann J & Myllylä R (2008) Monte Carlo calculations of UV protective properties of emulsions containing TiO₂, Si and SiO₂ nanoparticles. *Proc. SPIE* 7022: 702211–1–7. DOI: 10.1117/12.804096.

Original papers are reprinted with permissions from SPIE (I–III, V, VII), Institute of Physics Publishing Ltd (IV), and Turpion-Moscow Ltd (VI).

Original publications are not included in the electronic version of the dissertation.

ACTA UNIVERSITATIS OULUENSIS
SERIES C TECHNICA

287. Elsilä, Ulla (2007) Knowledge discovery method for deriving conditional probabilities from large datasets
288. Perkkiö, Miia (2007) *Utilitas* restauroinnissa. Historiallisen rakennuksen käyttötarkoituksen muutos ja funktionaalinen integriteetti
289. Nissilä, Mauri (2008) Iterative receivers for digital communications via variational inference and estimation
290. Toivonen, Tuukka (2007) Efficient methods for video coding and processing
291. Lyöri, Veijo (2007) Structural monitoring with fibre-optic sensors using the pulsed time-of-flight method and other measurement techniques
292. Stoica, Lucian (2008) Non-coherent energy detection transceivers for Ultra Wideband Impulse radio systems
293. Koski, Anna (2008) Applicability of crude tall oil for wood protection
294. Gore, Amol (2008) Exploring the competitive advantage through ERP systems. From implementation to applications in agile networks
295. Kirillin, Mikhail (2008) Optical coherence tomography of strongly scattering media
296. Tölli, Antti (2008) Resource management in cooperative MIMO-OFDM cellular systems
297. Karkkila, Harri (2008) Consumer pre-purchase decision taxonomy
298. Rabbachin, Alberto (2008) Low complexity UWB receivers with ranging capabilities
299. Kunnari, Esa (2008) Multirate MC-CDMA. Performance analysis in stochastically modeled correlated fading channels, with an application to OFDM-UWB
300. Särkkä, Jussi (2008) A novel method for hazard rate estimates of the second level interconnections in infrastructure electronics
301. Mäkelä, Juha-Pekka (2008) Effects of handoff algorithms on the performance of multimedia wireless networks
302. Teräs, Jukka (2008) Regional science-based clusters. A case study of three European concentrations
303. Lahti, Markku (2008) Gravure offset printing for fabrication of electronic devices and integrated components in LTCC modules

Book orders:
OULU UNIVERSITY PRESS
P.O. Box 8200, FI-90014
University of Oulu, Finland

Distributed by
OULU UNIVERSITY LIBRARY
P.O. Box 7500, FI-90014
University of Oulu, Finland

S E R I E S E D I T O R S

A
SCIENTIAE RERUM NATURALIUM

Professor Mikko Siponen

B
HUMANIORA

University Lecturer Elise Kärkkäinen

C
TECHNICA

Professor Hannu Heusala

D
MEDICA

Professor Olli Vuolteenaho

E
SCIENTIAE RERUM SOCIALIUM

Senior Researcher Eila Estola

F
SCRIPTA ACADEMICA

Information officer Tiina Pistokoski

G
OECONOMICA

University Lecturer Seppo Eriksson

EDITOR IN CHIEF

Professor Olli Vuolteenaho

PUBLICATIONS EDITOR

Publications Editor Kirsti Nurkkala

ISBN 978-951-42-8897-5 (Paperback)

ISBN 978-951-42-8898-2 (PDF)

ISSN 0355-3213 (Print)

ISSN 1796-2226 (Online)

